

Scanning laser-induced breakdown spectrometer for mine walls

Ilkka Laine

School of Electrical Engineering

Thesis submitted for examination for the degree of Master of Science in Technology.

Espoo 27.05.2019

Supervisor

Prof. Jussi Leveinen

Advisor

Lasse Kangas

Copyright © 2019 Ilkka Laine(CC BY 4.0) This work is licensed under a Creative Commons Attribution 4.0 International License. <http://creativecommons.org/licenses/by/4.0/>

Author Ilkka Laine

Title Scanning laser-induced breakdown spectrometer for mine walls

Degree programme Automation and Electrical Engineering

Major Control, Robotics and Autonomous Systems **Code of major** ELEC3025

Supervisor Prof. Jussi Leveinen

Advisor Lasse Kangas

Date 27.05.2019 **Number of pages** 66+8 **Language** English

Abstract

A prototype stand-off scanning laser-induced breakdown spectroscopy (LIBS) device for mine wall imaging is designed, built and tested in practice. The hardware and software design of the prototype device and a brief analysis of first experimental results are presented. Introduction part reviews the theory and current applications of LIBS. The design choices are laid out in detail and evaluated in their advantages in disadvantages. The end result is a highly automated scanning measurement device, which is also tested in practical tests. The primary experimental results demonstrate the feasibility of a standoff scanning LIBS device in harsh mine conditions and great potential value in the elemental heatmaps acquired with the device.

Keywords LIBS, LIBS Lidar, Plasma Spectroscopy, Instrumentation, Remote Spectroscopy, Mining, Spectroscopy, Standoff LIBS, Instrument Control, Prototype Design, Laser-Induced Breakdown Spectroscopy, Prototyping, Geochemical Analysis, Geochemical Spectroscopy, Lidar, Remote imaging, Remote LIBS

Tekijä Ilkka Laine

Työn nimi Skannaava laser-indusoitu plasmaspektrometri kaivoskäyttöön

Koulutusohjelma Automaatio ja sähkötekniikka

Pääaine Sääntötekniikka, robotiikka ja autonomiset järjestelmät **Pääaineen koodi** ELEC3025

Työn valvoja Prof. Jussi Leveinen

Työn ohjaaja Lasse Kangas

Päivämäärä 27.05.2019

Sivumäärä 66+8

Kieli Englanti

Tiivistelmä

Työ esittelee kaivosseinämien kuvantamiseen tarkoitettua skannaavaa laser-indusoitua plasmaspektroskopiaa hyödyntävän prototyypilaitteen. Lopputuloksena on pitkälle automatisoitu skannaava mittalaitteisto, jonka toimivuus osoitetaan käytännön testauksella. Kokeellisina päätuloksina ovat todistus skannaavan laserspektroskopia-laitteen toimivuudesta kaivoksen vaikeissa olosuhteissa sekä laitteella tuotettujen alkuainekarttojen arvon osoitus.

Avainsanat laserspektroskopia, plasmaspektroskopia, etäspektroskopia, spektroskopia, kaivosteknologia, mittalaite, prototyyppi, laitesuunnittelu, geokemiallinen analyysi, geokemiallinen spektroskopia, spektrikuvantaminen, instrumentointi, laser-indusoitu plasmaspektroskopia, LIBS, lidar

Preface

This thesis is a compilation of the results of many months of work by not only me but many colleagues and other people supporting me and my work. I wish to thank my coworkers for their support every day and for good teamwork spirit. The original plans for this thesis were far too large and ambitious in scale, but thanks to guidance from my advisor we managed to squeeze it into the more essential parts and the work was finished. This text is still a bit too large in scope to go in depth analysis for all of the important and interesting details, but it tries to give all the essentials in an overview of this prototype building project. Following the principles of open research, the codes written, 3D models created and experimental data acquired during this project is published alongside this thesis on zenodo.org archive. I am proud to have this work finished and I hope the reader finds this text readable and interesting. The results themselves are very exciting and the device we built is not only a new type of powerful measuring device never built before but also a cool laser cannon.

Espoo, 27.05.2019

Ilkka Laine

Contents

Abstract	3
Abstract (in Finnish)	4
Preface	5
Contents	6
Symbols and abbreviations	9
1 Introduction	10
1.1 Goal	10
1.2 Research hypotheses	10
1.3 Use case diagram	10
1.4 ChemCam as a reference	11
1.5 Thesis structure	11
2 LIBS Background	13
2.1 Laser-induced plasma	13
2.2 Elemental lines	13
2.2.1 Element detection	14
2.3 Comparison of LIBS to other analytical techniques	15
2.4 LIBS applications	16
2.4.1 Standoff LIBS	17
2.4.2 LIBS in geological analysis and mining applications	17
2.5 Challenges and solutions in standoff LIBS	18
2.6 Optical configuration for standoff LIBS	19
3 Instrument control background	21
3.1 RS485	21
3.2 ModBus	21
3.3 USB: Universal Serial Bus	21
3.4 TCP/IP: Internet protocol Suite	21
3.5 VISA: Virtual Instrument Software Architecture	22
4 Background of methods	23
4.1 Distance measuring	23
4.1.1 Laser rangefinding	23
4.1.2 Inverse rangefinding	23
4.2 Laser beam autofocus	23
4.2.1 Autofocus method 1 using sound and light intensity	23
4.2.2 Autofocus method 2 using laser rangefinder	24
4.2.3 Autofocus fine tuning using sound and light intensity	24
4.2.4 Calibration of autofocus system using sound and light intensity	24
4.3 Acquiring a 3D Model of the target	24

4.4	Spectrum normalization	25
4.5	Classification methods and machine learning	26
5	Hardware	27
5.1	Main materials and devices	27
5.2	Optical system for laser focusing	27
5.3	Optical system for light collecting	28
5.4	Motorized scanning frame	28
5.5	Hardware connections	28
5.6	Microcontroller wiring diagram	30
6	Instrument control logic and software	31
6.1	Goals and challenges for instrument control	31
6.2	Control design	31
6.3	Timings and delay generation	33
6.4	Laser control details	34
6.5	Stepper motor control	34
6.6	Autofocus and autofocus calibration	34
6.6.1	Calibration data Gaussian fit	35
6.7	Scanning system	35
6.8	Scanning measurement logic	36
6.9	Software design	37
6.9.1	Hardware abstraction	37
6.9.2	Used software environment and tools	37
6.9.3	Graphical user interface for control	38
6.10	Visualization tools	39
7	Safety	40
8	Experimental tests and results	43
8.1	Kittilä gold mine samples test	43
8.2	Measured LIBS Spectra from Kittilä gold mine samples	43
8.3	Mineral samples test	45
8.4	Measured LIBS Spectra from sample minerals	46
8.5	Tunnel test	47
8.5.1	Rock types and minerals	47
8.6	Measured LIBS spectra from tunnel test	48
8.7	Classifying mine tunnel measurements	49
8.7.1	Found elements	50
8.8	3D model from rangefinder data	50
9	Discussion	52
9.1	Experimental tests summary	52
9.2	Answered research questions	52
9.3	Comparison to previous work	53
9.4	Experience on building and using a prototype device	53

9.4.1 Problems with the device	54
9.5 Future Work and Alternative designs	54
9.6 Acknowledgements	55
9.7 Source repository	56
References	57
A 3D models and printable parts	67
B Pictures of the prototype device	69
C Tunnel test results in detail	70

Symbols and abbreviations

Symbols

c	speed of light in vacuum $\approx 3.00 \times 10^8$ m/s
e	mathematical constant ≈ 2.72
k	Boltzmann constant $\approx 1.39 \times 10^{-23}$ J/K
m_e	electron rest mass $\approx 9.11 \times 10^{-31}$ kg
h	Planck's constant $\approx 6.63 \times 10^{-34}$ Js
π	mathematical constant ≈ 3.14

Abbreviations

3D	3-Dimensional
CF-LIBS	Calibration Free Laser-Induced Breakdown Spectroscopy
CPD	Coherent Point Drift
DOI	Digital Object Identifier
GUI	Graphical User Interface
ICP	Iterative Closest Point
KC	Kernel Correlation
LA-ICP-MS	Laser Ablation Inductively Coupled Mass Spectrometry
LIBS	Laser-Induced Breakdown Spectroscopy
LIF	Laser-Induced Fluorescence
LIPS	Laser-Induced Plasma Spectroscopy
LSS	Laser Spark Spectroscopy
lidar	Light detection and ranging
MPU	Multilevel Partition
NIST ASD	National Institute of Standards and Technology Atomic Spectral Database
Nd:YAG	Neodymium-doped Yttrium Aluminium Garnet
PCA	Principal Component Analysis
PCL	Point Cloud Library
PLA	Polylactic Acid
PLC	Programmable Logic Controller
POM	Polyoxymethylene
RPM	Robust Point Matching
SEM-EDS	Scanning Electron Microscopy Energy Dispersive Spectrometer
SVD	Singular Value Decomposition
SVM	State Vector Machine
TCP/IP	Transmission Control Protocol and the Internet Protocol
TPS-RP	Thin Plate Spline Robust Point matching
t-SNE	t-Distributed Stochastic Neighbour Embedding
TTL	Transistor-transistor logic
UMAP	Uniform Manifold Approximation and Projection
VISA	Virtual Instrument Software Architecture
WHAC	Wavelength Heatmap Analyzer with Click
XRF	X-Ray Fluorescence

1 Introduction

1.1 Goal

This thesis investigates the feasibility of stand-off laser-induced breakdown spectroscopy (LIBS) as a tool for geochemical analysis i.e. recognizing minerals and rocks. We build and present a prototype device capable of scanning a mine wall from 4 to 10 meter distance taking LIBS measurement from each point. The device needs to be mobile and it needs to withstand the harsh conditions in mine environment including vibration, sound, temperature changes, dust and moisture. The measurement and scanning needs to be fast enough for practical use in mining operations. The device needs to be not too expensive to build and needs to provide good data to be of interest to geological researchers and mining industry.

1.2 Research hypotheses

The research questions for this thesis are following:

- Hypothesis 1: LIBS light spectra can be used for classifying rocks and detection of minerals.
- Hypothesis 2: LIBS measurements can be localized in the mine system without too much difficulty.
- Hypothesis 3: A mobile standoff LIBS device capable of operating in the harsh environment in mines can be built.
- Hypothesis 4: Standoff LIBS device providing valuable information for mining industry or geological survey can be built.

Answers are provided in section [9.2](#).

1.3 Use case diagram

The use for our LIBS tunnel wall scanner is presented in an use case diagram in figure [1.1](#).

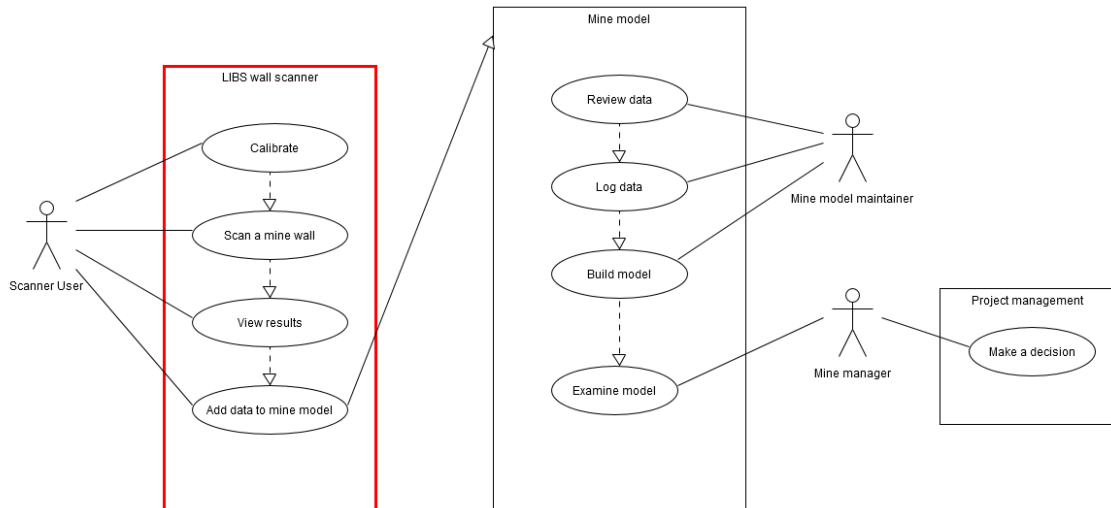


Figure 1.1: Use case diagram for LIBS tunnel wall scanner, device boundary is marked with a thicker line

1.4 ChemCam as a reference

The best documented and a good comparison for our device is ChemCam [1, 2] in the Mars Curiosity rover whose purpose is to analyze the elemental composition of soils and rocks on the surface of Mars. ChemCam design is explained in two papers by Maurice et al. [1] and Wiens et al. [2]. It does LIBS spectral analysis up to 9 meter distance and has a wide spectral range achieved using 3 separate spectrometers. ChemCam is a good comparison to what we are aiming for, allowing analysis from a distance and with a robust design working in harsh conditions and operating with high level of automation. For our application of a scanning device we need faster operation than the ChemCam allows, and we definitely need it much cheaper. To build a cheaper and faster version of ChemCam’s LIBS module would achieve the goals set for the hardware of this project.

1.5 Thesis structure

This thesis presents the design choices in both hardware and software for a LIBS tunnel wall scanner device, and the results acquired in the testing and building of the device. The main focus of this thesis, and the main contribution of the thesis author in this project, is on control and automation, on how to get the various parts of the device work as a one coherent whole as one easy-to-use measuring device.

The first part of the thesis, in order to understand the prototype device, explains the background of methods in three different sections: Section 2 describes LIBS via theory and its applications. Section 3 offers a technical background for instrumentation and protocols, and section 4 explains the background of technical and mathematical methods important for the function of the device and for making sense of the results.

Second part of the thesis presents the design of our device separated into two sections: section 5 for the hardware and section 6 for the control logic and software. System automation, integration and control along with the software considerations for each part of the system, are covered in this part. Section 7 is dedicated to safety considerations and has a preliminary list of safety rules made for the device.

The third part, section 8, describes experimental tests and measurement results obtained with the prototype device. This section together with the following discussion section will discuss the obtained results, and are the most interesting sections for readers who are not interested in the technical details but want to know what the device can achieve.

Finally, the discussion section 9 evaluates the acquired results comparing to previous work and considers possible improvements for the design and required future work.

Appendices contain extra results and photographs of the prototype device. Additional material including source codes, 3D model files and some acquired experimental results will be published alongside this thesis as described in section 9.7.

2 LIBS Background

Laser-induced breakdown spectroscopy(LIBS), also called laser-induced plasma spectroscopy(LIPS) or Laser Spark Spectroscopy(LSS), is an atomic emission spectroscopy method studied since soon after the first lasers were built [3]. To perform LIBS, laser is focused on the target to form a plasma spark and the light emitted by the plasma is then collected into a spectrometer. This light has a characteristic spectrum of atomic emission lines which allows detection and quantification of elemental content of the target. LIBS is a nearly non-destructive, so called micro-destructive method. LIBS can be performed on solid, liquid or gas. In this section an overview and theoretical principles of LIBS are presented.

2.1 Laser-induced plasma

The first working laser was built in 1960 by Theodore H. Maiman, and the interaction of laser with solids and the induced plasmas have been studied since [4]. Maker, Terhune and Savage were the first to report plasmas created by focused radiation from pulsed laser beams in 1963 [5]. Focusing a high power laser pulse on to a solid target causes intense local heating rising the surface temperature rapidly. A small amount, typically less than a milligram, of the material gets vaporized, dissociated and ionized forming plasma. For LIBS, ablation of around a few tens of nanograms of the target material is enough [6]. On solid materials, this forms an ablation crater with size and shape dependent on the material. Formation of high temperature plasma in atmosphere causes a pressure wave ie. sound, and cooling plasma emits light. The intensity of light emission is dependent on the temperature of the plasma and ambient air pressure. The plasma temperatures range typically from 5000 to 200,000 K [7]. The temperature is highly dependent on laser irradiance and thermo-optical properties of the target material. There is currently no complete physical model describing well the whole process of laser ablation [8]. [3, 8, 9]

Lasers of many different wavelengths can be used to induce the required spark, in or out of visible light range. Most commonly used laser wavelengths are 1064nm and 532nm corresponding to the very common Nd:YAG(Neodymium-doped Yttrium Aluminium Garnet) laser and its second harmonic.

2.2 Elemental lines

The excited atoms in the laser-induced plasma emit light at characteristic wavelengths and the intensity at each characteristic wavelength is dependent upon the number of atoms at a particular energy level. Therefore we can detect and quantify elements present in the plasma which correspond to the elements present in the target. We can calculate the energy state distribution of the atoms with Boltzmann equation and ionizations with the Saha ionization equation both of which are explained in this section. The physical behavior of the plasma is not totally known, but with some assumptions we can nevertheless make good approximations as to what shape of elemental spectrum to see from plasma.

Assuming local thermodynamic equilibrium, the relative numbers of atoms in each energy state at temperature T can be calculated with Boltzmann Equation (equation 1) [5].

$$\frac{N_B}{N_A} = \frac{g_B}{g_A} e^{\frac{E_A - E_B}{kT}} \quad (1)$$

Where N_A and N_B are the numbers of atoms, E_A and E_B the two energy levels, T the temperature in kelvin and k is the Boltzmann constant. g_A and g_B are the statistical weights for the two energy levels where $g_i = 2J_i + 1$ where J_i is the total angular momentum quantum number.

Another factor that affects emission lines is the number of atoms in different stages of ionization. This number can be calculated with the Saha ionization equation, also known as Saha-Langmuir equation, here equation 2. With generalized version of Saha equation, equation 3, we can calculate population of any ionization state.

$$\frac{N_+}{N_0} = \left(\frac{2\pi m_e k}{h^2} \right)^{\frac{3}{2}} \frac{T^{\frac{3}{2}}}{N_e} e^{\frac{-\chi_0}{kT}} \quad (2)$$

$$\frac{N_{j+1} N_e}{N_j} = \left(\frac{2\pi m_e k T}{h^2} \right)^{\frac{3}{2}} \frac{2Z_{j+1}(T)}{Z_j(T)} e^{\frac{-\chi_j}{kT}} \quad (3)$$

where N_j is population of the j :th ionization state, N_e is the electron density, Z_j is the partition function of the j :th ion and χ_j is the ionization energy of the j :th ion. The partition function Z_i is a weighted sum of the number of ways the atom can arrange its electrons with the same energy calculated by:

$$Z = \sum_{j=1}^{\infty} g_j e^{-\frac{E_j - E_1}{kT}} \quad (4)$$

Where g_j is the degeneracy factor which is the number of quantum states that have the same energy level.

In the equations, we find two factors that we have some control over: the temperature of the plasma T and the electron density of the plasma N_e . These are affected by the environment such as air pressure and the properties of the laser pulse, such as its length and energy, used to create the plasma. A change in these properties affects the relative population of the different ionization states and therefore the relative intensities of their emission lines.

Boltzmann and Saha equations alone do not explain the observed relative intensities of emission lines. Matrix effects, explained in section 2.5, complicate the situation. Optical properties of used optical components and absorption of ultra violet light by air must be also taken into account in our application. As stated before, the behaviour of laser-induced plasma is not completely known [8].

2.2.1 Element detection

Elements are identified from the LIBS spectra by identifying their elemental lines from the LIBS spectrum. As a good practice, at least three spectral lines should

be identified to positively identify an element [10]. These observed emission lines in the LIBS spectra can be compared to either in-house reference or to a standard database.

National Institute of Standards and Technology(NIST) in United States provides on their website a practical interface to their atomic spectral database(ASD) data to calculate emission lines for LIBS applications. NIST LIBS database uses Saha ionization equilibrium formulas and Boltzmann distribution function to calculate ion populations and element abundances, then radiative transition probabilities and the calculated level populations to obtain final spectral lines, and finally Gauss profile accounting to broaden the lines. [11]

For quantitative measurement of elements in LIBS spectra it is required to have either calibration data of known samples to compare to, or utilizing mathematical methods such as calibration-free LIBS(CF-LIBS) [12]. Determining isotope ratios with LIBS is possible with a high resolution spectrometer because of isotopic shift effect [13, 14].

2.3 Comparison of LIBS to other analytical techniques

Compared to other analytical techniques the good qualities of LIBS are the speed, easiness, relatively low investment, being almost non-destructive and ability to measure all elements simultaneously. On the other hand many LIBS applications are not ready technology and LIBS is still mostly non-quantitative and even though quantitative methods exist they can be difficult to implement and undeveloped [15].

Other analytical methods are listed in table 2.1 with a comparison to LIBS. Compared to other elemental analysis methods listed in the table, LIBS is easier to implement. [16] There has been considerable research in combining LIBS with other complementary laser based analytical techniques such as Raman spectroscopy [17–21] and Laser-induced fluorescence [22–26]. The advantage is combining the elemental information from LIBS with molecular information from LIF or Raman spectroscopy and because the instrumentation required is mostly the same a combined analysis is convenient to make [27].

Table 2.1: Analytical techniques

Elemental analysis method	Comparison to LIBS
Laser ablation inductively coupled plasma mass spectrometry(LA-ICP-MS)	High sensitivity
X-ray fluorescence(XRF)	Difficulty detecting lightest elements
Scanning electron microscopy energy dispersive spectrometer(SEM-EDS)	Requires sample preparation
Non-elemental analysis method	Information value
Raman spectroscopy	Molecular structural fingerprint
Laser-induced fluorescence(LIF)	Molecular structure and detection of species
Hyperspectral imaging	Spectral fingerprint

2.4 LIBS applications

LIBS is efficient in detecting even trace amounts of elements and a major application and research area for LIBS is detection of dangerous agents such as contaminants, explosives, chemical weapons or nuclear materials. LIBS is capable of detecting all elements in solids, liquids and gasses so it is a very versatile technique, with large number of application areas. The measuring equipment can be made simple and small enough to be made portable and fitting for in situ measurements. Selected examples of previous applications of LIBS along are listed in table 2.2. This list is only a small fraction of all LIBS applications under active research and development. As a relatively new technology and LIBS is to be expected to become more used measurement technique in future. [28]

Table 2.2: Some previous LIBS applications

Application	Examples
Detecting weapons of mass destruction(WMD) threats	Determining isotope ratios of nuclear material [29]
Detecting explosives	Detection and classification of explosive residues [30–32]
Detecting chemical agents	Rocket fuel and chemical warfare agent identification [33]
Detecting biological agents	E.coli identification [34, 35]
Analysis of food	Wheat grain analysis [36], identification of meat species [37]
Metal production process analysis	Determining steel sheet coating thickness [38]
Analysis of soil	Carbon measurement of soil [39, 40]
Biomedical applications	Detection of caries [41], cancer diagnosis [42]

2.4.1 Standoff LIBS

Remote LIBS in open path configuration is called standoff LIBS. First remote LIBS application was demonstrated in a paper from 1983 using laser for elemental analysis of airborne particles [43]. LIBS can be performed from a long range, demonstrated most clearly by Stelmaszczyk et al. in an article [44] from 2004 with a method for very long range LIBS measurement taking advantage of femtosecond lasers and laser filamentation in air. The technique was demonstrated up to a 90 meters away, and the authors expect it to be extendable up to kilometer range. Detailed information about open path LIBS can be found in a comprehensive review by Sallé et al. in 2007 [45].

A remote imaging or scanning LIBS device, named LIBS lidar, was reported first by Grönlund et al. in articles in 2005 [46] and 2006 [47] with the optical setup better described in a paper by Weibring et al. [48]. A patent US7692775B2 [49] by Treado et al. from 2010 describes a time and space resolved standoff lidar for explosives detection and includes LIBS as one of the sensing techniques.

2.4.2 LIBS in geological analysis and mining applications

There is some previous work evaluating the possibilities of LIBS for geological or mining applications. They are comprehensively reviewed in the articles by Qiao et al. in 2015 [10], Giorgio S. Senesi in 2015 [27] and Harmon et al. in 2013 [8]. In conclusion, LIBS shows great promise for analysis of geological materials and has been demonstrated to work in multiple applications, but further research is required to optimize the performance and capabilities of LIBS.

Getting from elemental to mineralogical information is a great challenge. There is no simple method to determine the mineral even if we managed to calculate the

accurate proportion for each element. This is for multiple reasons, firstly that different minerals can have identical elemental composition and secondly because often there is a mix of multiple minerals in the sample, even in the microscopic amount ablated in LIBS with a focused laser. More detailed analysis of the challenges is provided in the next section 2.5.

Thesis [15] by Khajehzadeh in 2018 and its related publications [50–52] focus on the mineral identification problem and consider LIBS for online mineral identification on drill cores and tail slurries. An advantage of LIBS is that it can be integrated in multiple phases of the mining process. LIBS analysis can be done for mine walls, on drill cores, for slurry or any other material flows in mining. Therefore it could be used both in mineral exploration phase and for process control during production. Both the input and output material of many mining processes could be analyzed with LIBS. Implementing LIBS analysis in mining processes could give valuable information on factors such as ore grade and environmental impact of mine tailings.

There are some existing products and companies doing LIBS-analysis for mining industry collected in table 2.3.

Table 2.3: Example companies and products for LIBS in mining

Company	Product	Target
Outotec	Outotec Courier 8 SL analyzer [53]	Online measurement of elemental content in plant feed, tailing and concentrate slurries
Elemission	Mission:Coriosity LIBS scanner [54, 55]	Elemental imaging of drill cores
Laser Distance Spectrometry	Maya online analyser [56]	Online analysis of elemental composition
IVEA Solution	EasyLIBS [57]	Handheld LIBS device for solid materials

2.5 Challenges and solutions in standoff LIBS

There are multiple challenges in standoff LIBS related to the distance and to the many different types of target material and environments of each application area.

Mezzacappa et al. [58] found that LIBS signal emission lines do not behave consistently with distance. This is a significant challenge for our measurements, making quantitative analysis of elements more difficult.

Chemical matrix effects occur when an element present in the material changes emission behavior of another, typically by inhibiting the ionization of an element with lower ionization potential. Physical matrix effects are more complex than chemical ones. An example of a physical matrix effect is how the material properties such as crystallinity or surface texture affect the quantity of ablated mass. [8]

Self absorption is the effect where light emitted by an element in the plasma is

then absorbed by the same element in another part of the plasma. Self absorption decreases intensity of an emission line proportional to the lower energy level in the energy transition responsible for that line [59].

Methods to successfully compensate for self-absorption and matrix effects have been developed such as previously mentioned CF-LIBS and multivariate analysis techniques like principal component regression analysis and partial least squares regression analysis. [60,61]

Lopez et al. recognizes in their article [62] that one of the main drawbacks to achieve analytical methods with laser ablation techniques is the great heterogeneity of environmental samples. Because of this the LIBS measurement from a single point of a sample can be a bad representation of the whole sample. In order to obtain a representative statistical sample using point analysis, a large number of measurements must be taken and subjected to statistical or geostatistical analysis.

The extra challenge for standoff LIBS applications are the environmental conditions for each application. The presence of water has been found to affect LIBS considerably. [62]. Presence of dust, dirt or other unwanted material on the samples can spoil the results by contaminating or masking the wanted signal. In some applications the target can be cleaned from moisture and dust by ablating the same spot more than one time with a laser pulse before the spectral measurement is recorded, for example Lui et al. [16] used five cleaning shots to remove dust and contaminants when measuring natural rocks.

A particular challenge in mining applications of LIBS is the harsh conditions inside the mine. Moisture, vibration, dust, changes in temperature and dangerous environment requires a lot from the equipment. The instrumentation setup must be resistant and robust enough to withstand and operate in these conditions. The instruments must be able to withstand and work reliably in a wide range of conditions including a wide temperature range. However, LIBS has been proven to work reliably in very difficult conditions in the space missions such as ChemCam explained in section 1.4.

2.6 Optical configuration for standoff LIBS

The optical system required for LIBS analysis consists of two main parts: (1)The optics to focus the laser beam, and (2)the optics for plasma light collection. They can in large part follow the same optical path and thus be part of the same configuration, or they can be completely separate. There is a wide variety of different optical systems used in LIBS applications.

Sallé et al. review of stand-off LIBS from 2007 [45] lists the different optical configurations used for stand-off LIBS analysis. The approximated maximum ranges allowed by optical setups to focus the laser beam for LIBS according to the review are listed in table 2.4. Different receiver optics used for LIBS are listed in table 2.5.

Table 2.4: LIBS focus optics ranges

Optics	Range	Example
Single lens	6 meters	[63]
Two or three lens system	60 meters	[46]
Galilean telescope	100 meters	[63]
Self-guiding filaments	up to many kilometers	[44]
Schmidt-Cassegrain telescope	9 meters	[1]
Herschelian telescope	up to hundreds of meters	[64]
Concave mirror	7.5 meters	[65]
Keplerian telescope (for LIBS in liquids)	5 meters	[66]

Table 2.5: LIBS receiver optics alternatives

Light collecting optics
Off-axis lens
Off-axis mirrors
Pierced mirror
Newton telescope
Dichroic mirror
Quartz plate
Maksutov-Cassegrain telescope

3 Instrument control background

Instrument control or instrumentation control refers to the logic of how the individual measuring instruments i.e. sensors and actuators are integrated and used in configuration of a larger system. Controller refers to a device that manipulates other devices and components to control the system parameters. Controller can be for example a microcontroller, computer or programmable logic controller(PLC).

Instrument control software can be a dedicated computer program, such as LabView, or a program written in a general programming language such as C. A book "Instrument control with Matlab" [67] lists benefits and drawbacks for both of these options. In conclusion, a general programming language allows better performance and versatility with the cost of more development and testing required.

In order for multiple components to work as one whole, the communication between these components must be possible. The communication protocols and standards for instrumentation help achieve and guarantee reliable communication and operation. Here we review those that were used during this project specifically RS485, USB, Modbus and TCP/IP. We also look at as common standard for instrument control: Virtual Instrument Software Architecture(VISA).

3.1 RS485

RS-485 standard, officially ANSI TIA/EIA-485(American National Standards Institute Telecommunications Industry Association / Electronic Industries Alliance Recommended Standard), defines electrical characteristics of a serial communication protocol. RS-485 supports data rates up to 10 Mbit/s and distances up to 1200 m. RS-485 uses three-state logic and allows linear bus topologies where multiple devices can be connected in series using only two wires. [68]

3.2 ModBus

ModBus is a serial communications protocol published in 1979 by Modicon. It is a common means to connect together industrial electronic devices and is a royalty-free industry standard. ModBus enables communication between multiple devices connected in the same network. [69]

3.3 USB: Universal Serial Bus

Universal Serial Bus(USB) was originally released 1996 and provides specifications for the connection between personal computers and their peripherals. More specifically it defines the requirements for cables, connectors, connection protocols, communication and power supply for these devices.

3.4 TCP/IP: Internet protocol Suite

The internet protocol suite, known as Transmission Control Protocol/Internet Protocol(TCP/IP), combines multiple networking protocols and provides end-to-end data

communication. It gives specifications on how data is packetized, addressed, transmitted, routed and received. The internet protocol suite is essential for transporting messages in the internet.

3.5 VISA: Virtual Instrument Software Architecture

Virtual Instrument Software Architecture(VISA) is an industry standard for an application programming interface for communication with measuring instruments. It provides the specifications for the interface between hardware and software such as device drivers and software development environments such as LabVIEW. For software developers VISA specification allows a developing multi-vendor software programs so that the VISA-compliant hardware instruments can be interchangeable with other VISA-compliant instruments. [70]

4 Background of methods

This section explains methods and some explored alternatives in our approach to create a stand-off LIBS device and analysis of LIBS data. Important for the measurement itself is the autofocus for which different methods are presented in section 4.2 and distance measuring covered in the following section 4.1. Section 4.3 is about building the 3D-model of the scene. Sections 4.4 and 4.5 are about the mathematical methods to analyze and visualize the measurement results. Methods for automation and instrument control are the topic of section 6.

4.1 Distance measuring

4.1.1 Laser rangefinding

Laser rangefinding is a distance measuring technique utilizing a laser beam to measure the distance to an object. There are three main alternative technologies to how a laser rangefinder works:

1. Time of Flight: measuring the time a laser beam takes to travel to the target and back. The total distance is simply speed of light times time travelled divided by two: $s = \frac{c\Delta t}{2}$.
2. Multiple frequency phase shift: Uses multiple frequencies and measures the phase shifts. The distance is then calculated from the phase shifts.
3. Interferometry: measuring the interference pattern of two or more light waves. The interferometry method is better suited at measuring small changes in distance rather than absolute distances [71].

4.1.2 Inverse rangefinding

Another option is to focus the system first using other methods such as the light or sound intensity as a marker, then inversely calculate the distance using known optical parameters such as the focal lengths of the lenses and the distances between them.

4.2 Laser beam autofocus

4.2.1 Autofocus method 1 using sound and light intensity

To find the best focus, we exploit the fact that sound and light signal intensity tells how well the laser is focused: the higher the intensity, the better the focus is. First we set the focus to infinity or as far as possible. Then we reduce the focal length while shooting with the laser until the sound or light signal from the laser is at its highest.

Laser focusing with a microphone has been done before by Barnett et al. [72]. The paper describes focusing method using the sound from a shock wave induced by

a laser spark. The sound is recorded with a microphone connected to an oscilloscope. Their application was shown to work at a 20 meter range.

4.2.2 Autofocus method 2 using laser rangefinder

Distance from laser to target is measured using a laser rangefinder. The focus is set to the calculated distance based on known optical parameters.

4.2.3 Autofocus fine tuning using sound and light intensity

The above methods can be combined by using sound and light intensity measurements to fine tune the focus after a rough focus with some other method such as method 2.

4.2.4 Calibration of autofocus system using sound and light intensity

Another way to combine methods 1 and 2 is to use method 1 to calibrate method 2. The optimal focus points for each distance measure are recorded and saved as a calibration curve. After calibration the optimal focus can be calculated with the distance measure and saved calibration curve. This is the method utilized in our device, both for focus and receiver optics. A drawback of this method is the time and effort required for calibration.

4.3 Acquiring a 3D Model of the target

High accuracy positioning of measurement points is very important for our application. Value of the measurement data for mining purposes is directly linked to how precisely its position is known. The goal in mind is to combine the acquired measurement data with a larger mine model used in the decision making process of the mining operations. This section reviews the methods for point cloud 3D scene building, which is one method to combine local measurement data with larger models.

3D point cloud data can be collected with a lidar or other rangefinder device. Our device collects the 3D location data simultaneously when scanning, as this information is also needed for the autofocus of the device. This data is used both to produce a 3D model of the scene, and for the distance calculations required for the focusing of the LIBS laser beam. Each LIBS measurement point result can be tied to the measurement coordinates to build a 3D model of the elemental composition in the rock layers.

There are two steps in building a 3D surface from the collected point cloud data. First step is combining the data from separate measurements into a single point cloud or a single model. Second step is building a 3D surface model from the point cloud.

Combining point clouds requires aligning the points from separate point sets correctly. This is called point set registration or point matching. There are many known algorithms for point set registration [73]. Most well known and most used is the iterative closest point(ICP) algorithm introduced by [74]. Other methods include:

robust point matching RPM, Thin plate spline robust point matching(TPS-RP) [75], Kernel correlation(KC) [76] and coherent point drift(CPD) [77].

For building a surface 3D model from the point cloud there are two main classes of methods: Those of (1) computation geometry: powercrust [78] and so called (2) implicit functions: Poisson surface [79], Hoppe surface [80] and Multilevel partition(MPU) [81]. Implementations of these algorithms exist in many free(libre) software packages, including but not limited to The Point Cloud Library(PCL) [82], CloudCompare [83] and MeshLab [84].

4.4 Spectrum normalization

This section presents normalization methods for improved detection of the significant features and better comparisons between signals. The methods are from the field of signal processing or statistical signal processing. We focus on a few common and mathematically simple normalization methods used in this project and name a few more sophisticated methods from the literature for LIBS spectral processing.

A simple normalization method is to make the total sum of all spectrum values equal to 1 by dividing each value with the sum of all values as is shown in equation 5.

$$x' = \frac{x}{\sum x} \quad (5)$$

Min-max normalization is a feature scaling method for scaling the values to be between 0 and 1. Min-max value is obtained by subtracting the minimum value and dividing with the difference of the maximum and minimum value as shown in equation 6.

$$x' = \frac{x - \min(x)}{\max(x) - \min(x)} \quad (6)$$

Z-score value is calculated by subtracting sample mean and dividing with the sample standard deviation as in equation 7, where z is the z-score, μ is sample mean and σ is sample standard deviation. A z-score value tells how many standard deviations the value differs from the mean.

$$z = \frac{x - \mu}{\sigma} \quad (7)$$

More sophisticated and application specific normalization methods also exist. Paper by Wang et al. [85] presents a method to normalize the spectrum based on the plasma temperature. Paper by Najarian et al. [86] present a new method for subtracting the continuum from a spectrum. Subtracting the continuum makes the elemental lines more visible and comparable.

One factor to consider when doing normalization is the amplitude of noise in the signal, as normalization methods can amplify the noise. Another factor is the distance to target since signal intensity is inversely proportional to the square of distance. Parameters of the plasma, especially the electron temperature and density, may also need to be taken into account.

4.5 Classification methods and machine learning

The analysis of multiple spectra, or any multidimensional data, can be thought of as a classification or regression problem. Multidimensional data can be made simpler with dimensional reduction methods and feature projecting methods.

Common methods for dimensional reduction are Principal component analysis (PCA) and Singular Value Decomposition (SVD). SVD has been used for LIBS mineral identification by Khajehzadeh et al. [50]. Newer more sophisticated and powerful methods for dimensional reduction and data visualization include t-Distributed Stochastic Neighbor Embedding (t-SNE) [87] and Uniform Manifold Approximation and Projection (UMAP) [88].

Clustering methods group together objects most similar to each other and are good tools for classifying observations. A commonly used clustering method is K-Means clustering which groups data into clusters where each observation belongs to a cluster with a mean value closest to the value of the observation. With many different clustering algorithms and implementations, the interpretation of the clusters produced by such an algorithm may be difficult. The result of a cluster analysis needs to be validated, as it is often easy to find artificial groups in data produced by a specific clustering method itself.

Support vector machine (SVM) is a learning model that separates data into two regions where the distance between the closest data points between the regions is maximized. After being constructed with labeled training data, SVM can classify new data points to the closest existing category. Liang et al. [89] demonstrates the use of SVMs for LIBS steel material classification.

Neural networks can be used as a classification method for LIBS analysis. A neural network is trained using a training algorithm and a training dataset and after the network has been trained it is used as a classifier for new data. Neural networks have been used for LIBS analysis in several applications and have been demonstrated to accurately classify geological samples. [16, 90]

Methods utilizing neural networks with more layers than in so-called classical machine learning are called deep learning methods. Deep learning can produce efficient classifiers but generally requires a larger training dataset than classical methods. Deep learning methods might be a good solution for LIBS analysis in the future, but currently there is not enough data available to efficiently use deep learning for LIBS geological analysis. An example of deep learning neural network applied to spectroscopy is in a recent paper by Ghosh et al. [91] where the authors used molecule structure to predict excitation spectra of organic molecules.

5 Hardware

This section presents the overall design and hardware for our tentative device applied for a proof-of-concept test of the principle of our stand-off LIBS scanner. Figures 5.1 and 5.2 show the basic foundation for our design. Extra detail and a concrete view on the device are in the appendices B for photographs and A for 3D models.

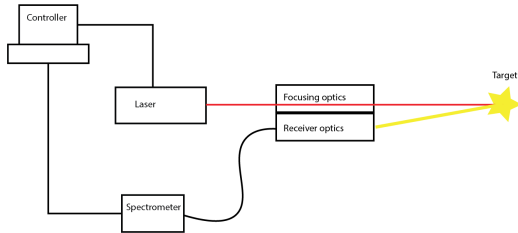


Figure 5.1: Design chart

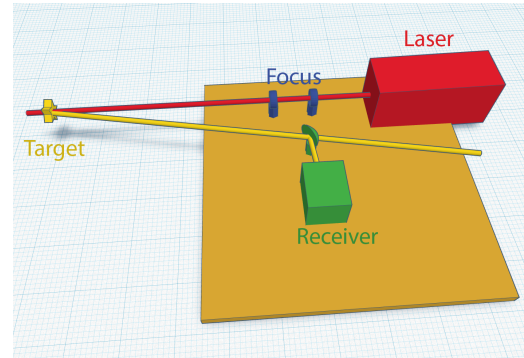


Figure 5.2: Design model

5.1 Main materials and devices

Materials used in building were polylactic acid (PLA) for 3D-printed parts, polyoxymethylene (POM) technical plastic for CNC-machined parts, and plywood for the box frame to make the device mobile. The optical components, the main plate, and other parts are from the selection of Thorlabs and Edmund Optics. The laser was Quantel Q-Smart 450 Nd:YAG (Neodymium-doped yttrium aluminium garnet: $\text{Nd}^{3+}\text{Y}_3\text{Al}_5\text{O}_{12}$) Q-switched laser with 1064 nm wavelength, 5 ns pulse length, 20 Hz frequency and pulse energy adjustable up to 400 mJ. Spectrometers were BWTEK Exemplar LS and Exemplar miniature CCD spectrometers with wavelength ranges of 200–400 nm and 350–1050 nm. As controllers we used Arduino Mega 2560 microcontroller and a Dell Latitude rugged laptop.

5.2 Optical system for laser focusing

The focus system consists of two lenses: one dispersing lens of -30 mm focal length and one focusing lens of 200 mm focal length. The dispersing lens, which is first on the optical path, is mounted on a linear positioning stage powered with a stepper motor which is controlled with a microcontroller. Moving this stage changes the distance between the two lenses and allows controlling of the focal length of the optical system. The laser is shot through these two lenses which focus the laser to a set distance. An autofocus system keeps the focal point of the lens system at the measured distance to the target, keeping the laser always at focus when the distance to target is changed.

5.3 Optical system for light collecting

Primary component for light collecting is a 2 inch diameter and 6 inch focal length off-axis parabolic mirror(Thorlabs MPD269-F01), which focuses the light to an optical fiber bundle(Thorlabs BFL200HS02) connected to a spectrometer. In the current design this parabolic mirror is a short distance off from the optical path of the laser beam, which causes a problem that the focus point in reference to the light collecting mirror moves as the distance to the target changes. To compensate for this problem we built a system that moves the fiber optic end in relation with the focus optics to gather maximum amount of light. The fiber end is on a linear positioning stage powered with a stepper motor that is controlled with a microcontroller. This design requiring a moving receiver is a bit complicated and could be made obsolete with different optical design.

5.4 Motorized scanning frame

Device frame, which allows rotation in two direction, is depicted in figures 5.3 and 5.4. Seen in the figures is a linear actuator which enables the pitch direction movement for the device. This frame is put on a motorized rotary table, not shown in the figures, enabling yaw direction movement. Photographs with the built frame can be found in appendix B and the separate machined parts used in constructing this frame in appendix A.

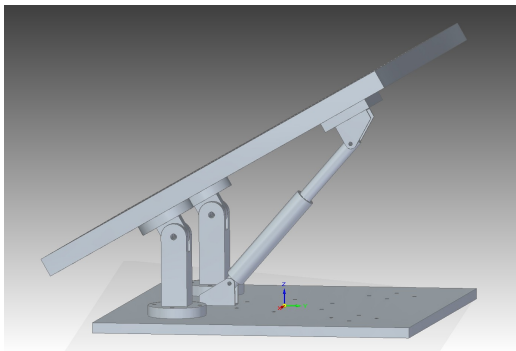


Figure 5.3: Prototype device rotating frame, upper position. Designed by Tuure Takala

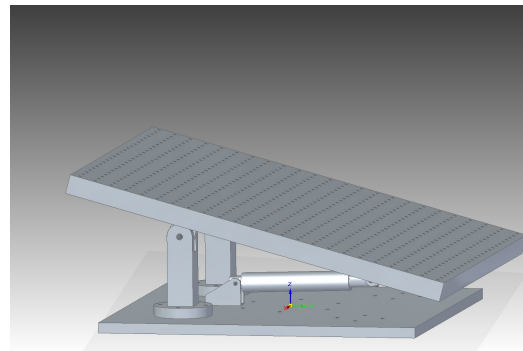


Figure 5.4: Prototype device rotating frame, lower position. Designed by Tuure Takala

5.5 Hardware connections

Figure 5.5 is a diagram of the different parts in the system and the connections between them. Each one of these connections is necessary for the device to work properly. From the figure we can count 13 connection paths or 18 connections if two-way connections are counted as two each. The connection type or protocol is marked next to each connection arrow in the figure. Information about these protocols can be found in background section 3.

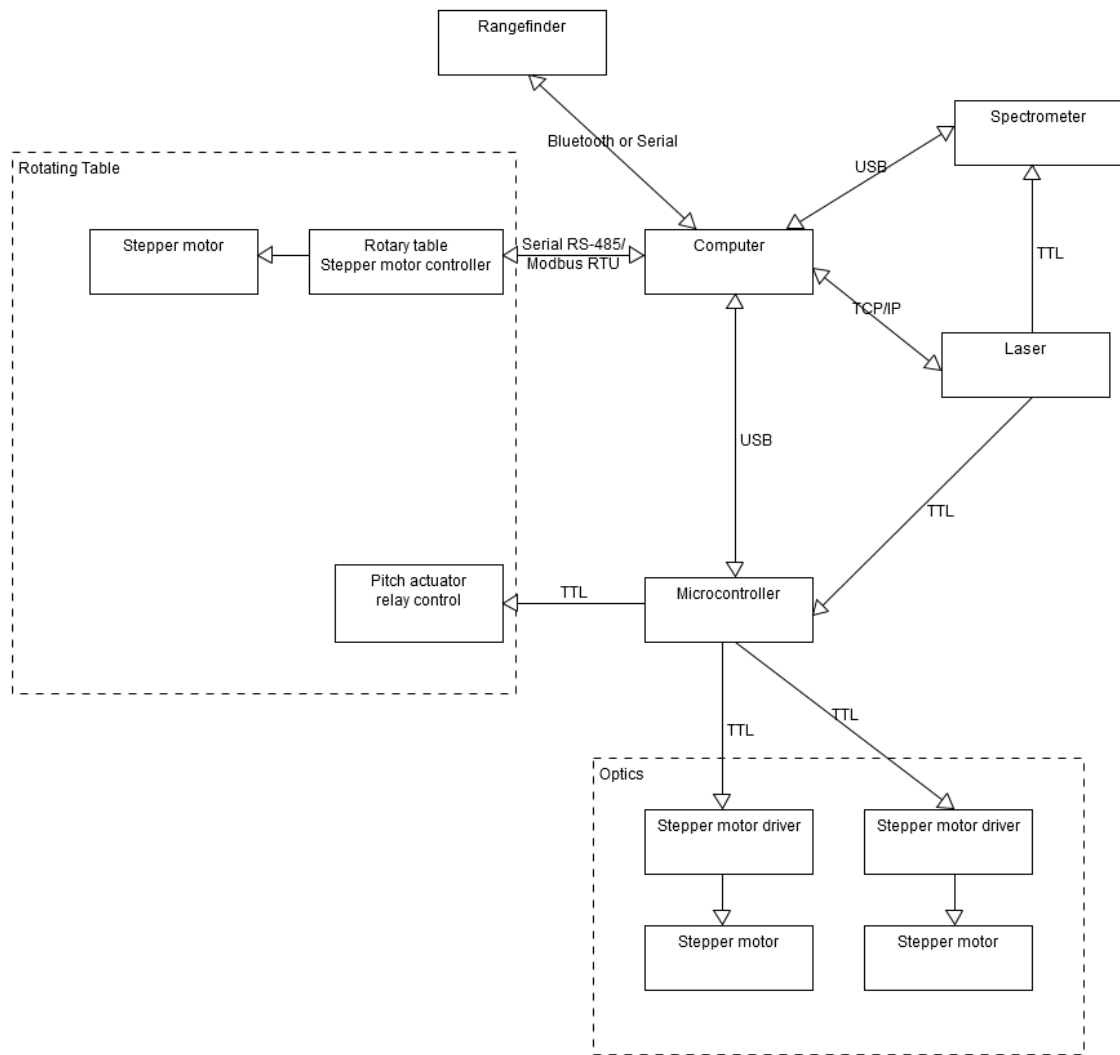


Figure 5.5: Device logical parts and connections

Figure 5.6 is a diagram of the power supply paths for the components. It shows for example, important for safety considerations, that to turn off the laser the power needs to be cut off from either the main power plug or from the laser power supply unit.

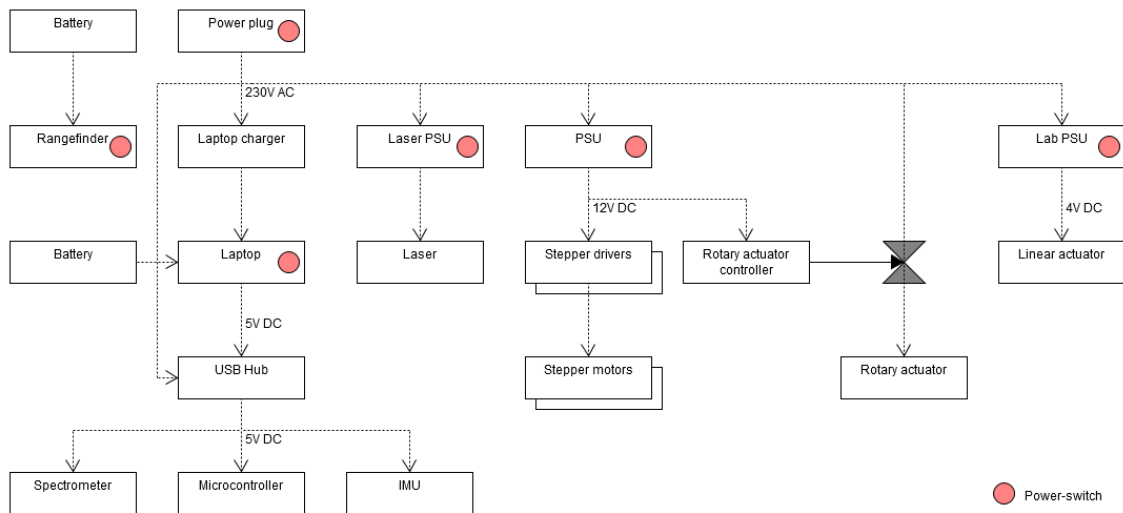


Figure 5.6: Power supply diagram

5.6 Microcontroller wiring diagram

The wiring diagram for components connected to Arduino Mega 2560 microcontroller is presented in figure 5.7.

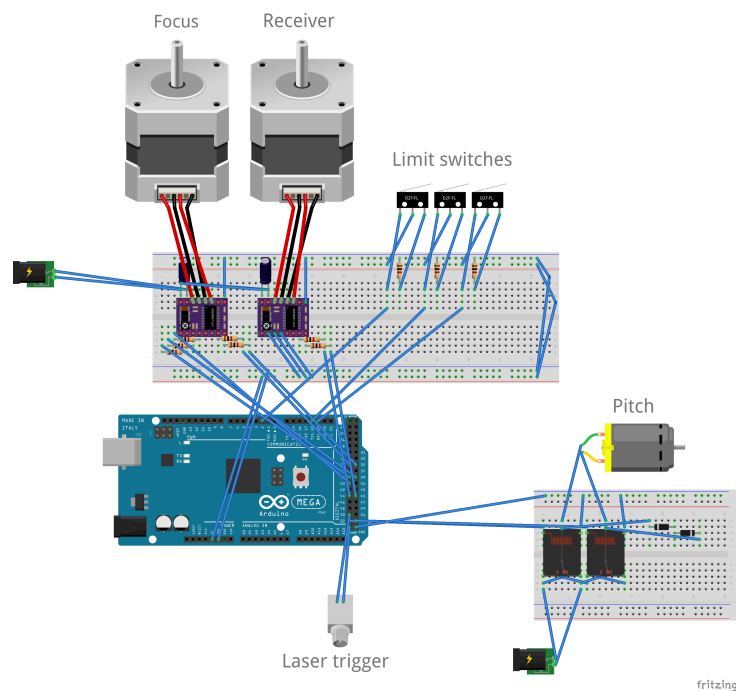


Figure 5.7: Wiring diagram for the microcontroller and connected components. The image was made with Fritzing, which is a free software tool for electronics design.

6 Instrument control logic and software

This section presents the control logic for the prototype device. In the prototype device, we have 4 motors, 3 sensors, laser, spectrometer and a microphone that must all be operated in a synchronized manner. Section 6.2 gives a big picture of the control using block diagrams to make a clear how each subsystem is controlled and to demonstrate control flow. Section 6.3 tackles an important issue in controlling a LIBS device, namely the synchronized timing of the laser and spectrometer. Sections 6.5, 6.6 and 6.7 each describe the control of one important part of the hardware: stepper motors, autofocus and scanning movement actuators. Finally section 6.9 describes the software design choices.

6.1 Goals and challenges for instrument control

Design of the control is the main focus and contribution of the thesis author during this project. Automated control was developed for each instrument as part of the control software for the device. The goal is that everything is controlled from a single computer interface and all gathered data is saved in the same directory with same identifying label. Parallel or simultaneous control of multiple instruments turned out to be an essential requirement with a device composed of this many components.

6.2 Control design

A control flow diagram demonstrating the logical separation of the device software is in figure 6.1. Some cross communication between these parallel components is required to keep them synchronized. To summarize the chart, first all devices are turned on and initialized, then the scan is carried out and lastly all devices are turned off and results are saved.

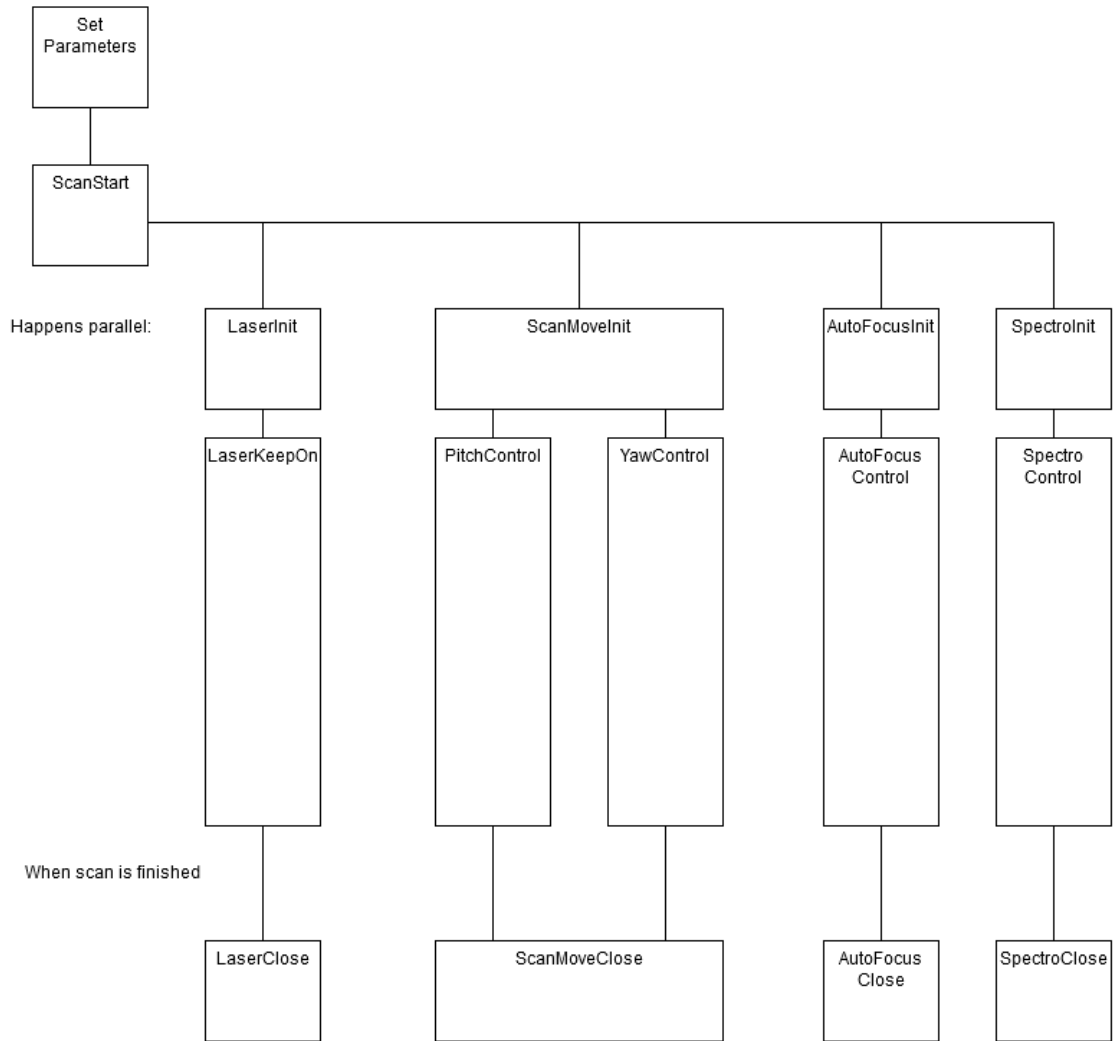


Figure 6.1: Control sequence diagram (logic flow)

Laser control is modelled with a simple open loop system in figure 6.2. In practice it turned out to be a bit more complicated requiring monitoring of the laser state and parameters but for its logical functioning in the system the open loop design is enough.

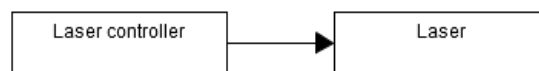


Figure 6.2: Laser control block diagram

The optics control system i.e. the autofocus system in figure 6.3 has two actuators, one for the focusing optics controlling the lens distance and one for the receiver optics controlling the position of the receiver. Both are controlled by the same reference value given by a distance sensor. The target value is calculated from the reference value according to a calibration curve created in the calibration phase described

in section 6.6. The optics control is an open loop except for a safety feature of limit switches on the edges of the safe area for the actuators to ensure they are not accidentally driven too far.

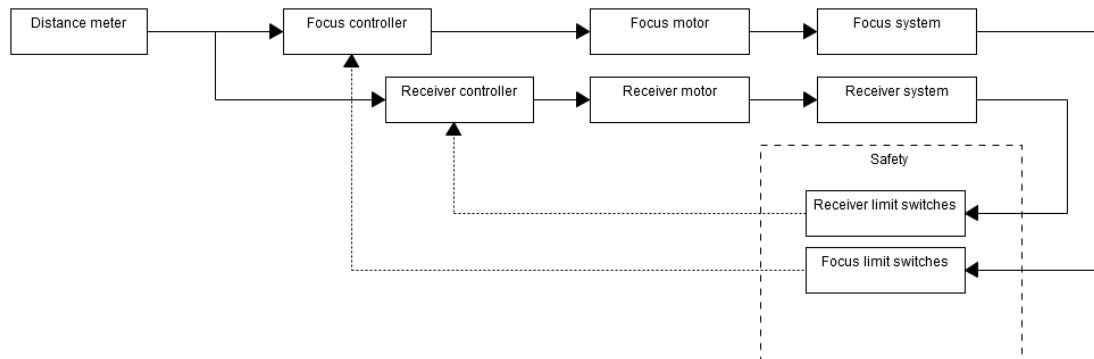


Figure 6.3: Optics control block diagram

The angle control consists of one angle sensor and one motor in a closed loop with the controller which drives the motor as close to the reference angle as possible. The angle control is same for both yaw and pitch angle, so the system in figure 6.4 is doubled for controlling both angles.

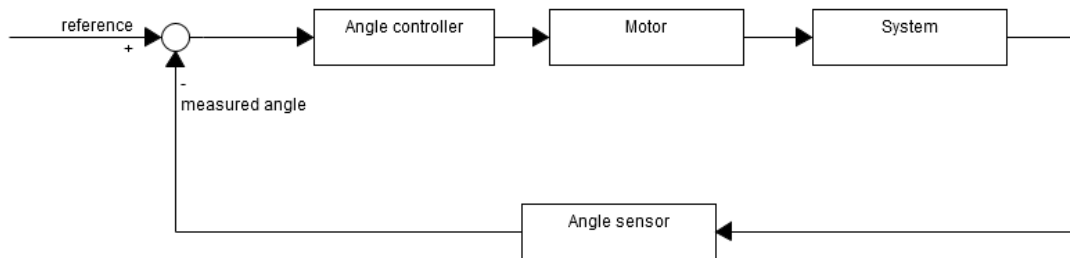


Figure 6.4: Yaw or Pitch control block diagram

6.3 Timings and delay generation

Laser-induced plasma is time evolving and therefore fine control of the time delay between laser pulse and exposure time of the detector can be needed. The more interesting light emission for in LIBS elemental analysis occurs some microseconds after the laser pulse, after the plasma has formed and is in the state of cooling down. Triggered-gated detection allows controlling these timings and is common in LIBS systems [92]. The trigger signal pulse can be generated by the laser, by a fast photodiode detecting the laser output or by an outside pulse generator used to trigger both the laser and the detector.

In practice we found that our spectrometers do not react fast enough to a trigger pulse sent at the same time as the laser pulse to be able to measure the wanted plasma signal as it dies within microseconds. By testing we found that the spectrometers we have had around 5 to 50 microsecond delay between the trigger pulse and measurement

window. A practical workaround we took advantage of is to shoot two laser pulses in succession for one measurement, using the first pulse only as a trigger and the second pulse for the LIBS measurement itself. For many purposes the LIBS signal can be good enough without fine timing by simply using integration times over the whole lifetime of the plasma.

6.4 Laser control details

We found out that our laser has an undocumented safety feature to turn itself off whenever a connection to the controlling computer is lost or any communications from it hasn't been received in a few seconds. Repeatedly polling the laser is thus required during operation. This was a surprise feature that we found out when developing code to control the laser.

6.5 Stepper motor control

The focus and receiver optics are driven by two stepper motors drivers (DRV8825, Texas Instruments, on a Polulu stepper motor driver carrier) controlled by a microcontroller (Arduino Mega 2560 Rev3), which was connected to a laptop computer. The microcontroller is powered with USB power and the stepper drivers get power from a 12V power supply unit salvaged from a personal computer. The control logic is Arduino code, which is C++ with some Arduino additions and to control the stepper drivers we used a MIT licensed StepperDriver Arduino library [93] by Laurentiu Badea.

6.6 Autofocus and autofocus calibration

The autofocus system controls the focusing optics and the receiving optics based on a distance measure. The target positions for the optics motors are calculated from a calibration curve generated before the LIBS measurements. The calibration curve itself is implemented in the form of a lookup table giving the relations between measured distance, optimal position for focus and optimal position for receiver. The calibration can be redone at anytime if necessary, but it should be only necessary when parts of the system are changed.

A method explained here and a supporting computer program was created for the calibration process. The autofocus calibration is done by generating a new calibration curve by doing calibration for multiple different distances. The method is as follows:

1. (User) Start the calibration program.
2. (User) A calibration target (an aluminium sheet) is set at a distance such that both the LIBS laser beam and distance measuring beam hit it.
3. (User) User presses "take a calibration point" button in the UI.
4. The distance to target is measured with a rangefinder and saved.

5. Microphone recording is turned on.
6. The LIBS laser is turned on.
7. Laser autofocus is driven to the point of best focus where the sound intensity is the highest. The focusing optics position is saved.
8. Receiver is driven to the point of best focus where the light intensity is the highest. The receiver position is saved.
9. Laser and microphone is turned off.
10. (User) Return to step 2 setting the target to new distance if more calibration points are required.

From the recorded values, distance and focus position constitute a point in the calibration curve for focus control. And likewise, distance and receiver position constitute a point in the calibration curve for receiver control.

6.6.1 Calibration data Gaussian fit

The raw calibration data constitutes of value-pairs of optics position and signal intensity, which is either sound or light intensity. To find out the maximum intensity point, we fit a Gaussian to the data and use the peak of the Gaussian as the maximum. The Gaussian peak value is less dependent on accidents and noise in the signal and is thus a more reliable value than a simple maximum over the values. It was tested experimentally to fit the data reasonably well but not perfectly. Figures 6.5 and 6.6 show an example of acquired calibration data and the fitted Gaussian curve.

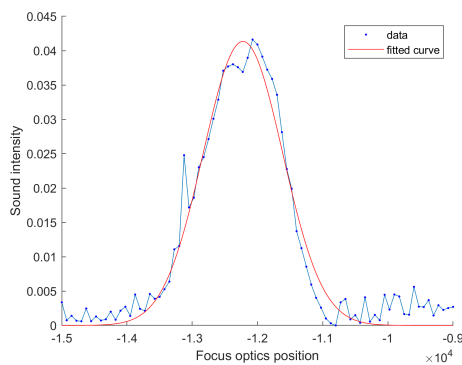


Figure 6.5: Gaussian fit on calibration data for focus position

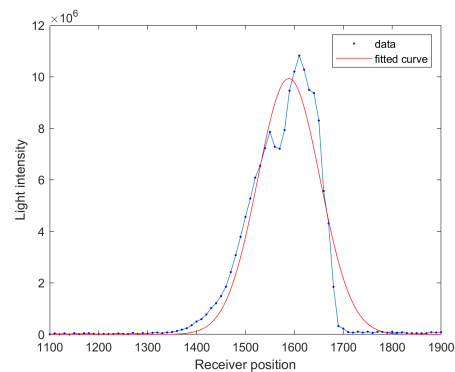


Figure 6.6: Gaussian fit on calibration data for receiver position

6.7 Scanning system

The laser and focus optics are mounted on a rotating and tilting table described in section 5.4. The system is designed to scan through a point set in the form of evenly spaced grid from the wall, but any arbitrary point set could be used. The controlled

variables are the angles, pitch and yaw of the table, which then correspond to a measurement point where the laser beam hits on the wall. Assuming a flat wall, the required angles for a wanted (X, Y) coordinate can be calculated using trigonometry as in equation 8. Same equation applies for calculating both yaw and pitch angles replacing the displacement with the displacement to x- or y- directions respectively.

$$\phi = \arctan\left(\frac{\Delta x}{d_0}\right) \quad (8)$$

Where ϕ is the angle, Δx is the displacement on the wall and d_0 is the distance from laser to the original target point. As an example we calculate the angles for evenly spaced points 10 centimeters apart on a wall from a distance of 5 meters we get results shown in table 6.1. When the displacement is small compared to the distance, the transform is close to linear i.e. with small angle we can use small-angle approximation.

Table 6.1: Relation of displacement at target and starting angle

displacement(meters) Δx	angle(radians)	angle(degrees)
-0.2	-0.400	-2.291
-0.1	-0.200	-1.146
0	0	0
0.1	0.0200	1.146
0.2	0.0400	2.291
0.3	0.0599	3.434
0.4	0.0798	4.574
0.5	0.0997	5.711
0.6	0.1194	6.843

6.8 Scanning measurement logic

There are multiple possibilities in how the scanning movement can be implemented. Multiple options were experimented with but we ended up on the a setup where the rangefinder and LIBS laser are oriented so that the rangefinder is pointing forward of the LIBS laser and we can simultaneously measure LIBS from point Y and the distance measure for the next point Y + 1. The scanning loop with this logic is as follows:

- Step 1: Turn on LIBS laser with continous shooting.
- Step 2: Take distance measure for measurement point Y + 1.
- Step 3: Turn LIBS laser and set focus distance to point Y = Y + 1.
- Step 4: Take LIBS measurement for point Y.
- Step 5: (Simultaneously with step 4) Take distance measure for point Y + 1.

- Step 6: Go back to Step 3 unless scan is finished.

In the tunnel test explained in section 8.5 we did the scanning only left to right and aimed the rangefinder few measurement steps distance right from the LIBS laser, and took a distance measurement about once every three steps interpolating the shape in between those measured points. This was done because the distance measuring was relatively slow and was a limiting factor to the scanning speed.

6.9 Software design

This section explains software design choices made during this project. Our software design philosophy was primarily focused on fast prototyping and easy obtainability of results. We also tried to provide free software solutions wherever possible, but some devices unfortunately require proprietary drivers. Safety considerations, repeatability of results through extensive logging, budget limitations and reusability of parts for iterative changing of design guided our project.

Because concurrency is needed with some device choices, the software is designed to support parallel control of multiple instruments simultaneously. This was an extra challenge for the software design. Parallel control was built with two principle solutions: First, the control logic was split between a microcontroller and laptop computer and secondly, the control codes on the computer have parallel functionality achieved with MATLAB parallel computing toolbox.

The produced codes, mostly MATLAB codes and Arduino codes will be published at a Zenodo repository described in section 9.7.

6.9.1 Hardware abstraction

For good modularity and reusability, the hardware should be abstracted in the code separating the wanted actions from the device specific operation like communication protocols. This allows much of the software to be reused even if parts of the system are replaced with other components. However, less abstracted code is better for easy tweaking and also helps understand device specific functionality through more transparent code.

In this work we strived for modular reusable code, but in practice the actual used scripts tend to be of a nature of a single long scripted hacked together to work for one specific task. Part of the abstraction work is already done, and some of the code is reusable even if any single device is changed to another. But more abstraction and code refactoring should be done to make the code is more readable and reliable. At the moment much of the control logic code is still component specific.

6.9.2 Used software environment and tools

Most of the controlling programs were written in MATLAB. We were already using MATLAB to do modelling for the device so using MATLAB allowed us to stay with the familiar tools. MATLAB versions used were R2017b, R2018a and R2018b. Many of the MATLAB programs we wrote will work also on GNU Octave either as is or

with some changes. But some of the programs are easily translatable because of the use of MATLAB parallel computing toolbox and other MATLAB specific features. The downsides of MATLAB environment are high memory requirement, slow start-up time and it being proprietary i.e. not free software. Translating the control codes to Python, C or C++ is a possible project in the future.

A rugged laptop computer with Windows 7(64-bit) is used as the master controller and as the main user interface. Most of the codes work just as well on GNU/Linux, but some device drivers are not available or are proprietary and more expensive than the Windows equivalent. The BWTEK spectrometer control codes unfortunately require the proprietary drivers from BWTEK SDK.

6.9.3 Graphical user interface for control

A graphical user interface(GUI) was built for some parts of the controlling. The GUI can be seen in figures 6.7-6.10. It was designed to be usable with either touchscreen or mouse. The main feature enabling touchscreen friendly control is big and clear buttons. The GUI is also a prototype and is missing many features and is only a mockup in some parts. Nevertheless, it gives an idea how we envision the device controller UI could look and it proved useful in testing of the different parts of the system. We used this GUI in a touch screen capable laptop to control our device.

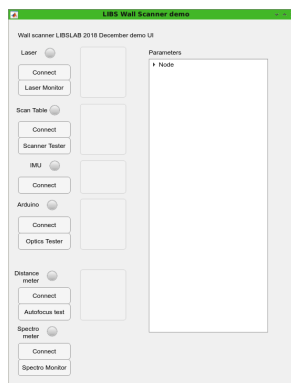


Figure 6.7: LIBS wall scanner GUI

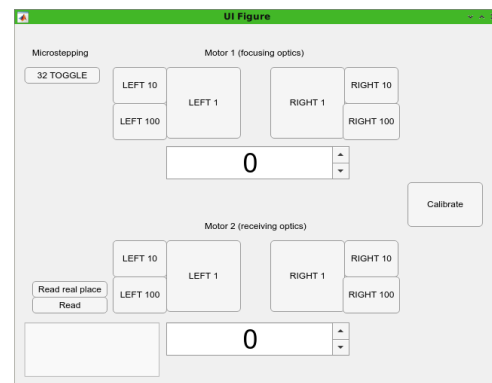


Figure 6.8: Optics control test GUI

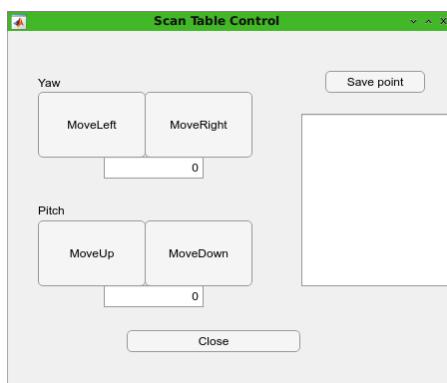


Figure 6.9: Scanner GUI

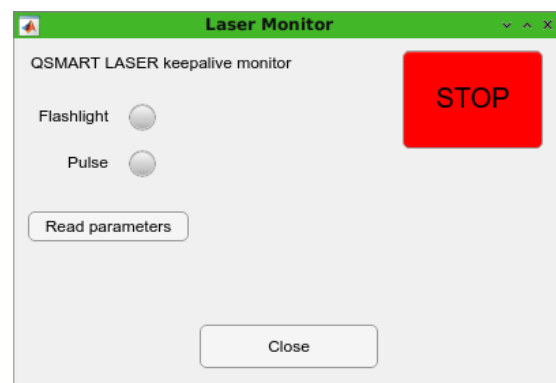


Figure 6.10: Laser GUI

6.10 Visualization tools

A lot of code in the form of MATLAB-scripts was written during this project to analyze and visualize the results. The built visualization tools were used to make pictures in the results section and in appendix C and for analysis of the results. We showcase here one of the tools built that we shall call Wavelength Heatmap Analyzer with Click or WHAC for short. WHAC is a two window app for looking at the spectral data produced by a LIBS scanner both in heatmap images and spectrum graphs. First window, depicted in figure 6.11, shows the heatmap image built with one wavelength and a slider to select the wavelength and a cursor to select any single pixel of the picture. Second window, depicted in figure 6.12, shows the complete spectrum of the pixel selected from the heatmap in the first window and the wavelength selected with a red line.

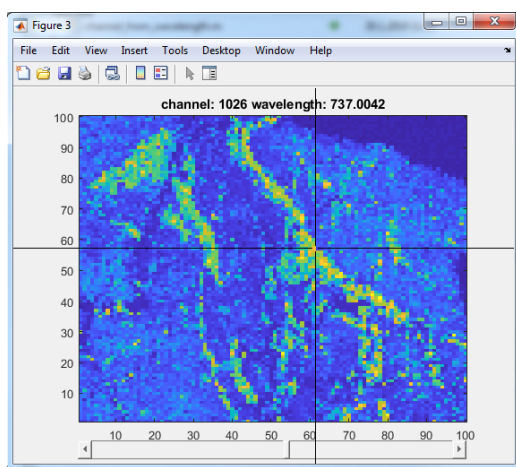


Figure 6.11: Wavelength Heatmap Analyzer with Click window 1

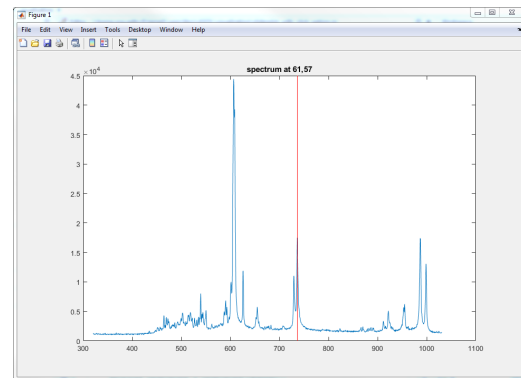


Figure 6.12: Wavelength Heatmap Analyzer with Click window 2

7 Safety

Because of the high power laser used, the system is potentially dangerous and may cause serious eye damage. Therefore the personnel using this device must take certain safety rules into consideration. This section presents an overview of the risk factors for personnel and equipment and lists rules of both design and operation to mitigate risks. Some rules that lead to good personnel safety also protect the device itself from damage and breaking.

Damage to eye induced by reflected or direct laser light is the primary danger in operating the device. The laser in the device is a 1064nm infrared laser, which is especially dangerous compared to visible light laser in two ways: 1. it is invisible to human eye which makes it hard to detect, and 2. it doesn't trigger the usually protective blink reflex. Furthermore, direct laser can also cause damage to skin but this is a minor consideration compared to the potential of serious eye damage. Other risk factors include the mechanical risk by the moving heavy equipment and possibility of electrical hazards.

Number one safety rule is to wear eye protection that protects from the specific wavelength of the laser device. The requirements for laser eye-protectors are defined by an European Standard EN 207:2017 also verified as the Finnish national standard SFS-EN 207:2017:en [94].

Proposed safety rules for users of the device are presented in table 7.1. Proposed safety considerations required from the software design are presented in table 7.2.

Table 7.1: Proposed safety rules

A user of the LIBS tunnelback scanner device must follow these safety rules:

- Always check and wear safety glasses that protect from the specific wavelength of the laser device.
- Warn others of invisible and potentially eye-damaging laser and make sure no one enters the area of potential hazard.
- Consider possible reflections of the laser. It can be dangerous even when not looked at directly and after multiple reflections.
- Do not enter in front of the laser during operation.
- Keep your hands off the device during operation.
- Before operation check that nothing is blocking the physical turning of the device.
- Check cable connections and battery level when applicable.
- Turn off the device in case of unusual or unexpected event.
- Turn off the device in case of unusual or unexpected operation.
- Follow laser safety rules.
- Follow location specific safety rules.
- Follow electrical equipment safety rules.
- Note: This list of rules is a draft for the prototype device and has not been reviewed by an expert.

Table 7.2: Proposed safety requirements for control software

Device control software should fulfill the following requirements:

- The instrument control must work reliably and safely.
- An important safety feature is to reliably turn off the laser in case anything unexpected happens.
- Obvious way to turn off the device.
- The UI should remind the user to wear safety glasses checked to offer protection from the correct wavelength.
- The UI should point out clearly when the laser is in operation and when it is turned off.

8 Experimental tests and results

The rest of this thesis is dedicated mostly to the experimental tests and results obtained with our prototype device. Here are documented three different tests in different kind of setup and on different target materials. Sections 8.1, 8.3 and 8.5 describe the measurement setups for the three tests and sections 8.2, 8.4 and 8.6 their results respectively.

8.1 Kittilä gold mine samples test

We took measurements from Kittilä gold mine samples. The samples used here are described in more detail by a colleague Konstantinos Bis in his thesis [95]. The main focus for these measurements was to find out how well we can detect arsenopyrite(FeAsS), which is the principal host of submicroscopic gold and thus mineral of interest in detecting the gold ore. To detect arsenopyrite we are interested mostly in the elemental lines of arsenic.

We had 50 samples, 32 of which were preclassified as 'ore' and 18 which were 'gangue'. Each rock sample was put on a rotating platform and a measurements series was taken from it. Each measurement series consists of 240 individual spectrum measurements, each of which is from a different spot due to the rotation of the sample. The laser was operated with 20 Hz frequency using 1 passive(no emission) and 2 active pulses for each cycle of 3 clock pulses. The actual measurement is taken with the second active pulse and the first is only used as a timing trigger. The total measurement time for one series was 36 seconds. Spectrometer used in this test was BWTEK Exemplar LS miniature CCD spectrometer with wavelength range of 200-400nm. Figure 8.1 shows an example sample where the burn mark made by the laser can be seen. The amount of arsenic in the samples was previously measured with a handheld XRF-device. The XRF-results are compared to our LIBS measurement and used as a validating reference.

8.2 Measured LIBS Spectra from Kittilä gold mine samples

Figure 8.2 shows an example spectrum obtained from a single point, figure 8.3 shows the mean spectrum over all measurement points in one sample and figure 8.4 shows the spectra of a full measurement series of 240 spectrum. Figures 8.5 and 8.6 show an example spectrum from an arsenopyrite shot. The many elemental lines of iron dominate the spectrum but at least one elemental line of arsenic is well visible and marked in figure 8.6. The number of LIBS shots that hit arsenopyrite was calculated using a simple treshold value for the intensity of a specific wavelength corresponding to a elemental line of arsenic. Figure 8.7 is a histogram of calculated number of arsenopyrite shots for each ore and gangue rock. If we were to reclassify the samples based on this figure, multiple of the 'ore' samples would be moved to a 'gangue' category and three of 'gangue' samples would be moved to 'ore' category. Figure 8.8 shows a comparison between XRF-measured arsenic and and the number of arsenopyrite shots with LIBS for those samples that were measured with both.

A linear fit was made to the data points and the coefficient of determination R^2 calculated to be 67%.



Figure 8.1: Kittilä Au mine rock sample with burn marks from 2 measurement series.

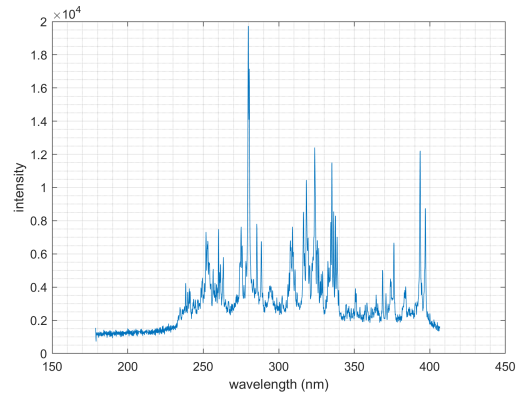


Figure 8.2: Kittilä Au mine rock sample single point spectrum measurement.

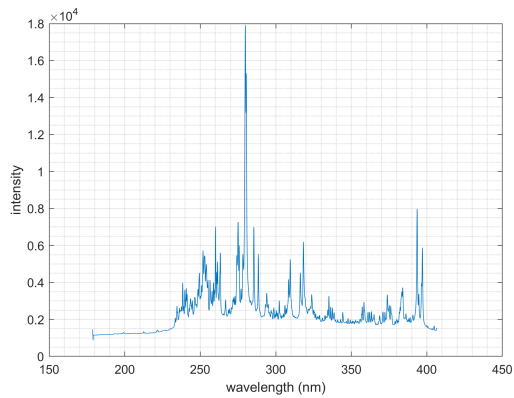


Figure 8.3: Mean spectrum from a measurement series around a Kittilä Au mine rock sample.

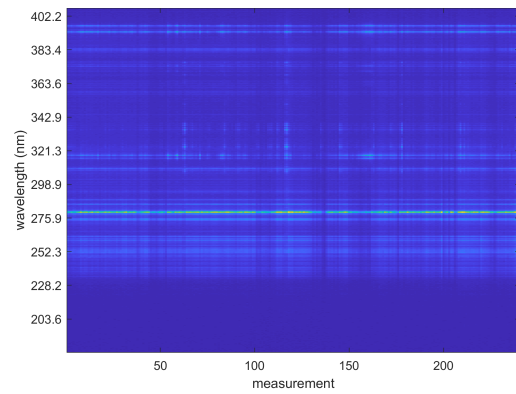


Figure 8.4: Spectrogram of a measurement series around a Kittilä Au mine rock sample.

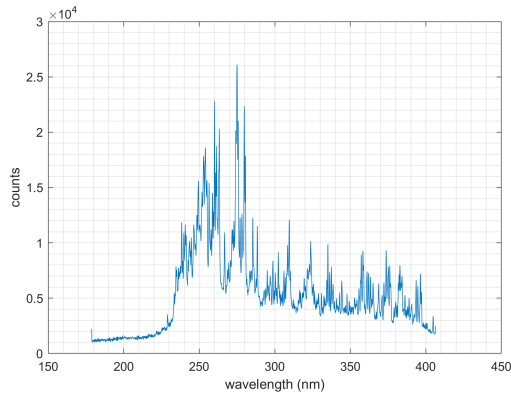


Figure 8.5: Kittilä Au mine sample test spectrum of an arsenopyrite(FeAsS) shot.

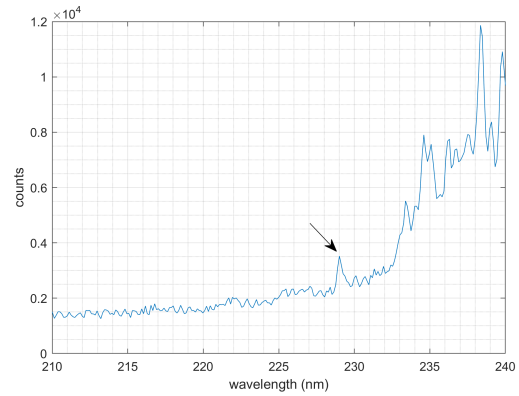


Figure 8.6: Kittilä Au mine sample test spectrum of an arsenopyrite(FeAsS) shot zoomed in with one characteristic arsenic wavelength 229 nm highlighted.

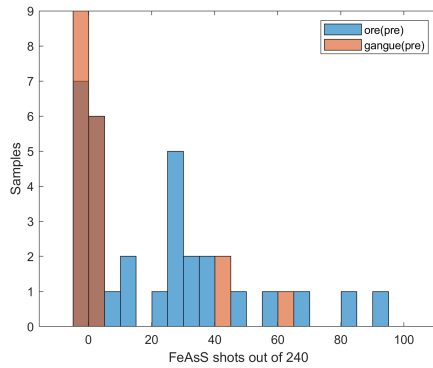


Figure 8.7: Arsenopyrite shots histogram of ore and gangue samples.

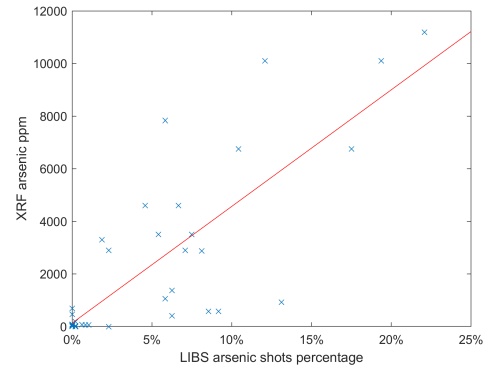


Figure 8.8: XRF measured As compared to LIBS arsenopyrite shots percentage

8.3 Mineral samples test

A set of pieces of different known mineral was laid on a metal plate next to each other and scanned through with the prototype device. The two goals for this test was first to verify the scanning system works properly and secondly to make sure that we can see in the results the obviously different minerals. The minerals from left to right and top to bottom as seen in figure 8.10 are magnetite, apatite ore(first), apatite ore(second), gypsum, beryl, dolomite, graphite, olivine, pyrite, serpentine and potassium feldspar. Figure 8.9 is a photograph of the test setup. Spectrometer used in this test was BWTEK Exemplar miniature CCD spectrometer with wavelength range of 350-1050nm.

8.4 Measured LIBS Spectra from sample minerals

The mineral samples test results are presented as elemental heatmaps. These heatmap images are constructed point-by-point by summing together the intensity of multiple identified wavelengths for each element. The elemental wavelength were identified and marked by hand from the resulted spectra with the help of NIST LIBS database [11] and previous experience with the spectrometer. The spectra were normalized to z-score values as explained in section 4.4. Figures 8.11-8.16 show elemental heatmaps of iron, calcium, sodium, magnesium, beryllium and phosphorus respectively. In the pictures dark blue means low intensity of the respective elemental line wavelengths and light yellow means high intensity.

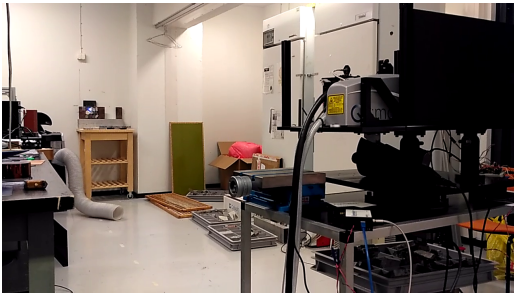


Figure 8.9: Mineral sample test setup photograph.

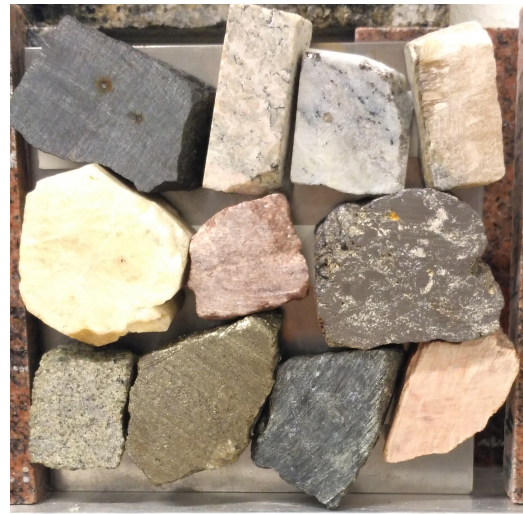


Figure 8.10: Mineral sample photograph.

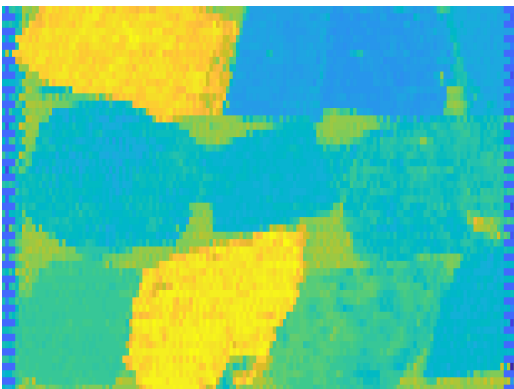


Figure 8.11: Mineral sample test elemental heatmap for iron.

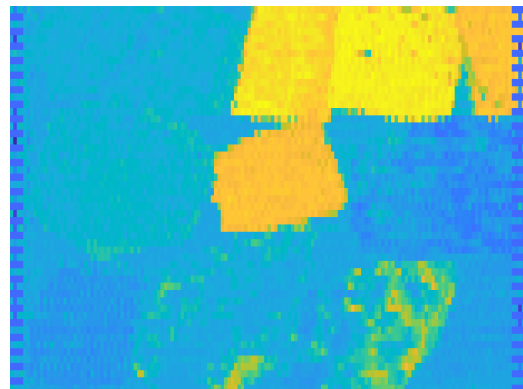


Figure 8.12: Mineral sample test elemental heatmap for calcium.

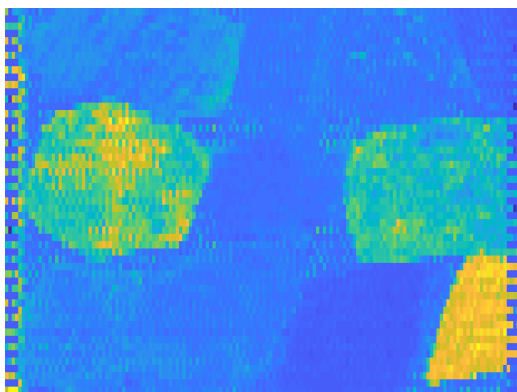


Figure 8.13: Mineral sample test elemental heatmap for sodium.

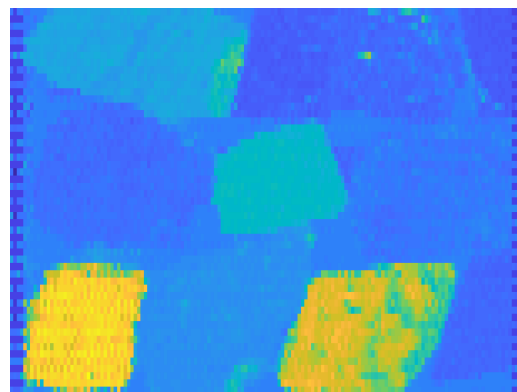


Figure 8.14: Mineral sample test elemental heatmap for magnesium.

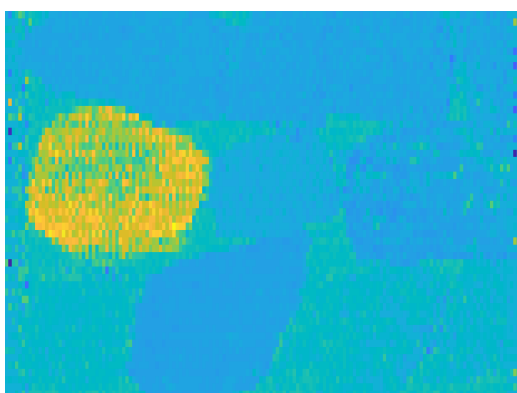


Figure 8.15: Mineral sample test elemental heatmap for beryllium.

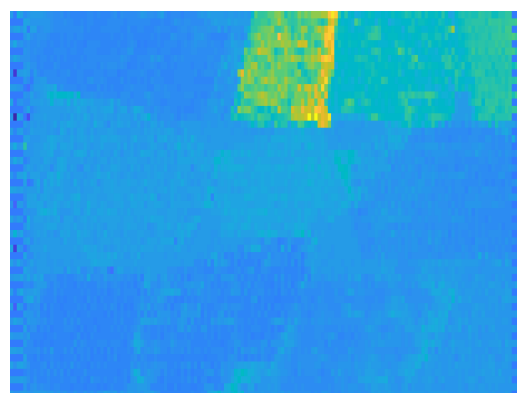


Figure 8.16: Mineral sample test elemental heatmap for phosphorus.

8.5 Tunnel test

To demonstrate that the device works in the required environment, a scan was done in a realistic mine like environment in underground research tunnel of Aalto University. Photographs of the target wall are in figures 8.17 and 8.18. Spectrometer used in this test was BWTEK Exemplar miniature CCD spectrometer with wavelength range of 350-1050nm.

8.5.1 Rock types and minerals

This section provides a very brief listing of the types of rock and minerals in the target wall. This is not a verified or complete analysis but its purpose is to give an idea of what the target wall is like. The measured wall is mostly granitic migmatite with medium to coarse grained granitic segregation part i.e, leucosome and darker subvolcanic like gneissic residual part i.e. melanosome. Minerals in the wall include feldspar group rock like plagioclase, mica group minerals such as biotite and muscovite, and hornblende.

8.6 Measured LIBS spectra from tunnel test

This section shows some of the results obtained in the tunnel test, more results are in appendix C. The scan was $300 \times 300 = 90000$ measurement points which took 5 hours of continuous scanning time. For each measurement point a LIBS spectrum was measured and for every two to three points also a distance measure which was used for the autofocus of the optics. Figure 8.22 shows the mean spectrum over all measurement points and figures 8.19 and 8.21 show elemental heatmaps visualised considering a elemental line intensity values, for calcium and sodium respectively. Figure 8.20 has the calcium elemental heatmap overlaid on top of a photograph of the area. In the pictures dark blue means low intensity of the respective elemental line wavelengths and light yellow means high intensity.



Figure 8.17: Photograph of the test location in tunnel wall test.



Figure 8.18: Photograph of the scanned area in tunnel wall test.

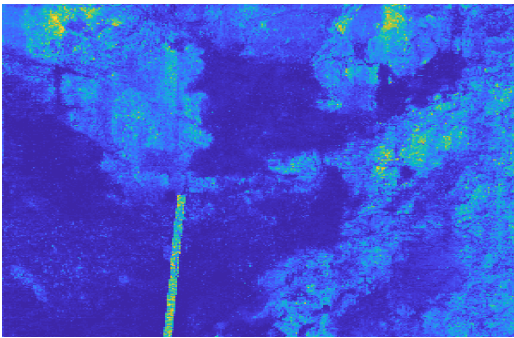


Figure 8.19: Tunnel wall elemental heatmap for calcium. Combined from multiple wavelengths.

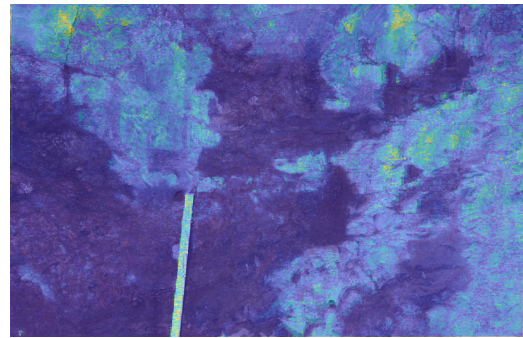


Figure 8.20: Tunnel wall elemental heatmap for calcium overlaid on top of a photograph.

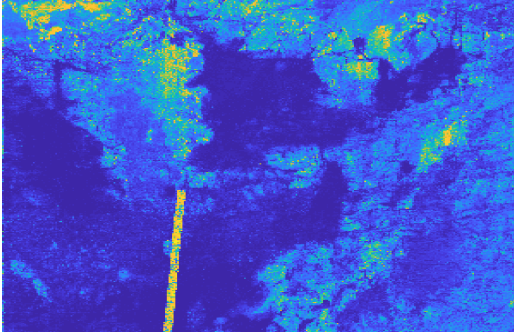


Figure 8.21: Tunnel wall elemental heatmap for sodium, combined from wavelengths 589.02 nm and 819.48 nm. Compare with the photograph in figure 8.18.

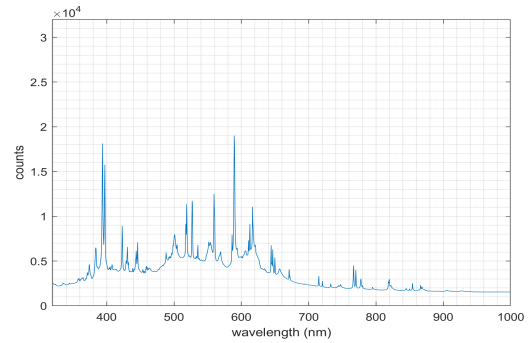


Figure 8.22: Tunnel wall mean spectrum

8.7 Classifying mine tunnel measurements

The wet parts differ very clearly from the dry parts as we can see in the heatmap figures 8.19 and 8.21. In figures 8.23 and 8.24 are example spectra acquired from a dry and clean part of the wall, and from a more dirty and very wet part of the wall. Comparing these two figures we notice that the signal acquired from wet surface is considerably worse with only a few elemental lines identifiable.

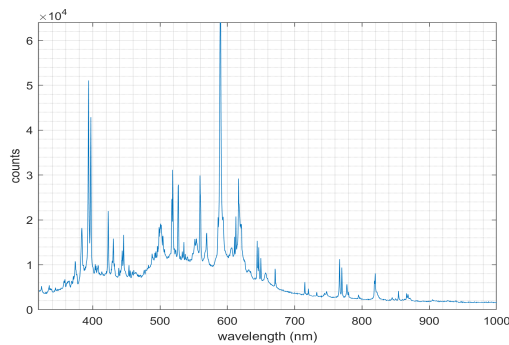


Figure 8.23: Example spectrum from dry part of the wall.

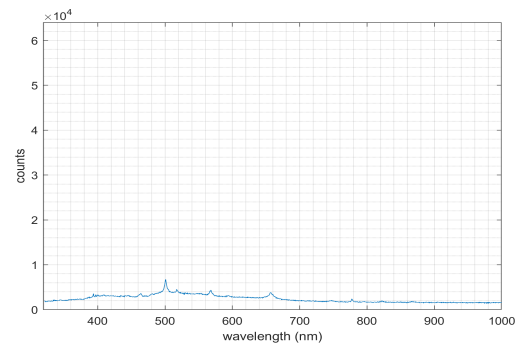


Figure 8.24: Example spectrum from wet and dirty part of the wall.

The dust in the environment significantly affects the results. The spectra obtained from aluminium plate used as a reference marker was highly altered by the presence of dust that had gathered on its surface. The aluminium plate also seem to work as a LIBS-amplifier, improving the overall intensity of the gathered spectrum also in spectral lines obtained from the dust. Comparison of the spectrums obtained from dusty aluminium and cleaned aluminium surface can be seen in figures 8.25 and 8.26.

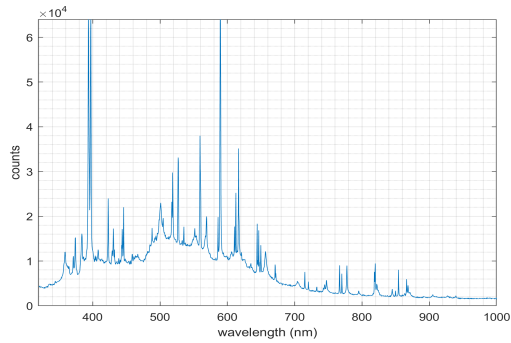


Figure 8.25: Spectrum obtained from a dusty aluminium surface.

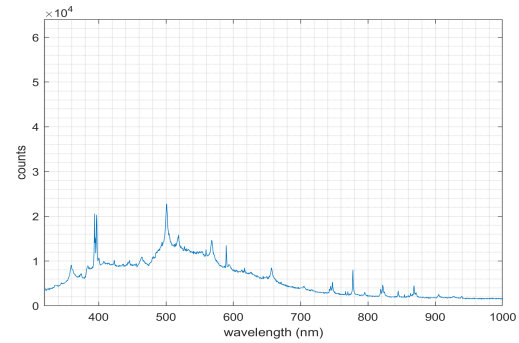


Figure 8.26: Spectrum obtained from a cleaned aluminium surface.

8.7.1 Found elements

This section showcases some of the identified elements and how they are located. The elements were identified by positively identifying two or more known elemental lines from the measured spectra. Manganese(appendix figure C14) was found most strongly on dried water trails. Rubidium(appendix figure C24) was identified and seems to be distributed similarly to potassium(appendix figure C10), which is expected as rubidium can replace potassium in minerals. Titanium(appendix figure C28) was identified in some points. Sodium(figure 8.21) and calcium(figure 8.19) are important markers of many minerals and abundant on the acquired pictures. Iron(appendix figure C8) was detected very strongly on a few single points. Oxygen(appendix figure C22) and nitrogen(appendix figure C20) are detected likely because of LIBS happening in air, especially from the wet areas where the LIBS signal was not good overall.

8.8 3D model from rangefinder data

The distance measure from laser to the target was captured every couple of measurement points. In figure 8.27 is a 3 dimensional model of the tunnel wall built from the distance and angle data acquired during the scan. The angle data is distorted from reality for two reasons, first the laser origin is not on the rotation axes i.e. the laser origin moves in space with the rotations, and second the two different directions, x and y or yaw and pitch, are not scaled correctly. The correct angles could be calculated with coordinate transformations using Denavit-Hartenberg parameters defined from the 3D model of the device or measured from the physical device itself. However, the distortion is small and not important for the purposes of this test so the calculations are omitted here. On top and bottom part of the model we see a lot of missing points which are missing because of technical difficulties(read: out of battery) with the rangefinder.

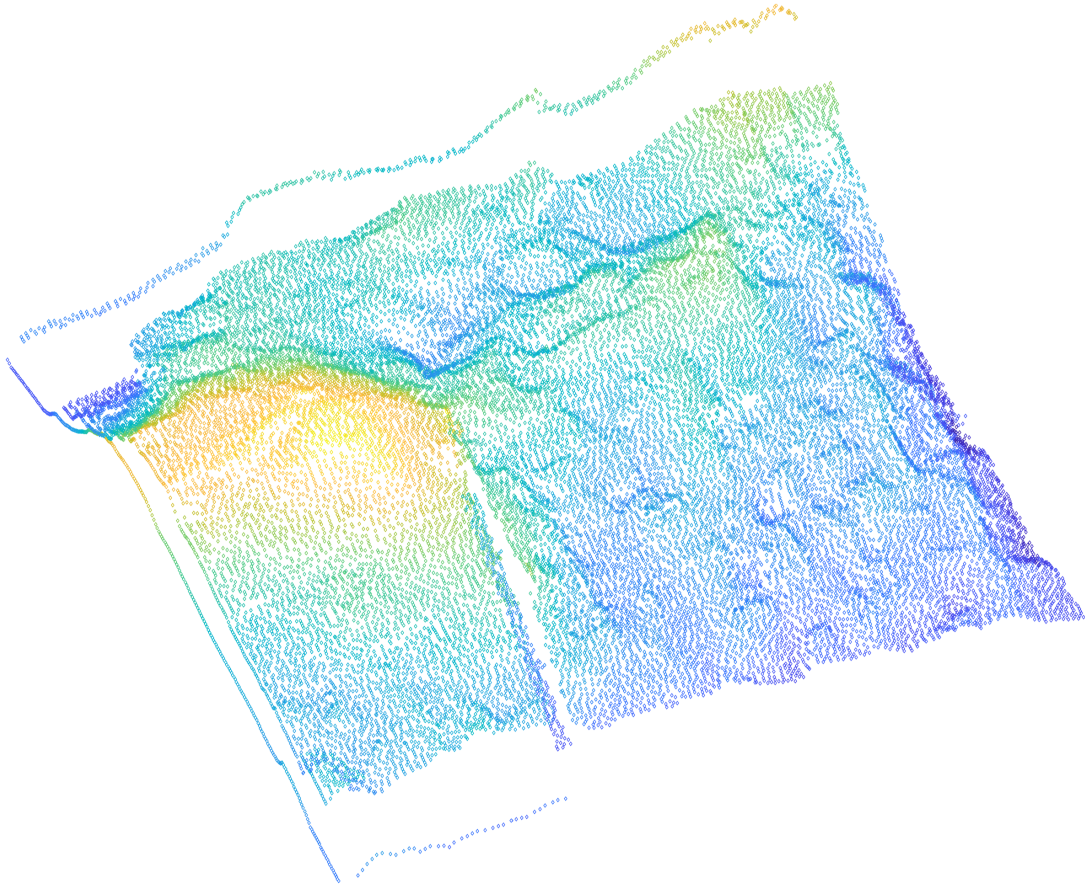


Figure 8.27: 3D-model point cloud of the tunnel wall constructed from rangefinder data.

9 Discussion

This thesis presented a device design for a mine wall LIBS scanner along with experimental results obtained with a prototype device. The built prototype device and results obtained with it show as a proof-of-concept that such a device is feasible and that it works well in the right conditions. The results obtained and the preliminary analysis on the data demonstrate the potential value of LIBS remote scanning analysis and also highlight challenges in in situ LIBS in mine conditions.

9.1 Experimental tests summary

The main experimental results of this thesis are the results of the three tests, each demonstrating different capabilities of a scanning LIBS device. The mineral sample test results demonstrate that we can detect multiple different elements with the LIBS scanner and that we can distinguish between these different minerals. The Kittilä mine samples test is a simple demonstration that our device is capable of obtaining valuable information in a real situation by showing that our device is capable of differentiating between the ore and gangue in this example case. The more comprehensive test was the tunnel test which demonstrates that the device works in realistic mine conditions and is capable of producing useful data in mine environment.

However, the presence of water and dirt seems to be a big problem for this type of LIBS scanner. The signal acquired from the wet parts of surface of the tunnel wall is significantly worse than from dry surface. Furthermore, the presence of dust affects the measurement significantly, sometimes more of the signal comes from the dust than the target itself. Future work is required to find out how significantly the dust affects the results and if its contribution could be effectively filtered. In earlier laboratory tests we had not noticed any problem with LIBS on wet rocks. But the tunnel test wall was a particularly challenging target in these regards because of the long time accumulation of dust mixed with the flowing water. The big adverse effect on signal quality seems to come from the mix of water and dust where there is a moist layer of dirt on the wall. These effects must be taken into account when interpreting the acquired spectra if the target is not carefully cleaned before measurements. Cleaning the target rock wall may be necessary before LIBS measurements. Some mines already include cleaning the tunnel walls as part of their process so it would not be an unreasonable demand.

9.2 Answered research questions

This section gives the found answers to the four research questions laid out in the beginning in section 1.2.

- Question 1 asked if LIBS spectra can be used to classify minerals and rocks. The results of the mineral sample test demonstrate hypothesis 1 **true**.

- Question 2 was about localizing the measurements in the mine. It was not completely addressed in this thesis but the produced 3D-model in figure 8.27 along with methods reviewed in section 4.3 with methods to stitch together 3D point clouds show that this problem can be solved with existing methods so hypothesis 2 is **true**.
- Question 3 asked whether a standoff LIBS device can handle the rough conditions in a mine, is answered **true** as demonstrated by the tunnel test.
- Question 4 answer is **true** demonstrated by all three tests together: our scanning LIBS device is capable of producing impressive and informative elemental-content maps allowing differentiation between different minerals or between ore and gangue.

9.3 Comparison to previous work

First scanning standoff LIBS device or LIBS lidar is described by Grönlund et al. in [46,47]. Compared to theirs our device is smaller, fitting in a back of a van instead of a truck. With the right components, especially a smaller laser, the device could be designed to be much lighter and smaller still. With 60 meter range their device had a longer range than ours, thanks to bigger optics in their device.

High resolution LIBS images made with smaller scale LIBS scanners have been published before e.g. by Caceres et al. in an article "Megapixel multi-elemental imaging by Laser-Induced Breakdown Spectroscopy" [96] in 2017. But our work, as far as we know, is the first time high resolution images from stand-off LIBS scanning are published.

The advantage of our solution to previously built portable LIBS devices capable of in situ measurement is the fast and automated remote imaging of a large area. Remote imaging stand-off LIBS systems have been built before, but our solution is the first stand-off LIBS device designed for scanning movement and producing high resolution images. Many previously built LIBS systems, including ChemCam, would be capable of acquiring similar results but would probably be either much slower or require manual operation if they were not designed for scanning movement like our prototype device.

9.4 Experience on building and using a prototype device

Our device in the end did what we wanted but with a lot of difficulties on the way. We experimented a lot with the optical setup but still ended up with a design that we are not really happy with. For the optics, a good-enough solution was selected. Many components worked unexpectedly and unexpected behavior and problems appeared in every stage of testing. The system consists of many parts and all the main components come from different manufacturers and with varying communication protocols and from different design philosophy. It was a lot of work with many experiences of unexpected problems and sometimes undocumented behaviour of a component on the way to get all the components to communicate together and work

in sync. Sometimes a big amount of trial and error was needed to fit a new component to the system.

When something we tested in the lab worked well enough, it was included in the design and when something didn't work we tried another solution. There is much to improve in the final design and some of the possibilities are discussed in sections [9.4.1](#) and [9.5](#).

After the tunnel test coming out of the tunnel back to daylight, we noticed our device was also completely covered in fine dust which we had not noticed in the dark tunnel. It proved us that the device can work fine in the dusty conditions, and luckily all our optic components were undamaged. It seemed that the laser pushed the dust away from the laser mirrors instead burning it on the surface damaging the component. Nevertheless the device would need a tight casing to protect it from dust, dirt and moisture.

9.4.1 Problems with the device

During the testing we encountered multiple problems with the device extending the duration our planned two day tunnel testing to a week as we had to retry multiple times and change the scanning logic a couple of times before we got all of the target area scanned with satisfactory results.

The electronics connections were not well made and sometimes caused problems with wires losing connection or causing the microcontroller to go in error state. Rangefinder device running out of battery was a problem in the tunnel tests. This was because we broke our rangefinder module a day before the tunnel tests and had to use a battery powered replacement during the tests. When some component in our device stopped working, it was often not clear what the problem was as our software did not produce detailed enough error messages. We utilized frequently the "Have you tried turning it off and on again" -approach. When something stopped working, turning off all power and restarting all devices including the control computer, usually fixed the problems. Better diagnostics and monitoring of the components would be required to pinpoint and fix all the problems encountered.

9.5 Future Work and Alternative designs

Some of our design choices, in hindsight, are not the best ones and there are many ways to improve the design. In this section we present improved, but unbuilt and untested, alternative designs for the device. A major change is to change the laser to a smaller one enabling the whole system much lighter and more mobile. The optics system can and needs to be improved with a better design allowing better focus on the target and thus reducing the needed energy of the laser pulses. A telescope based optics design would allow better focus and light gathering with longer distances as evidenced by the optics review in part [2.6](#). Dividing the signal with a splitting optical fiber bundle into multiple modular spectrometers is an option to gain better resolution or wider wavelength range. We experimented with modular spectrometers of two different wavelength ranges as can be seen for example in comparison of

figures 8.2 and 8.23. Combining these both into a wider wavelength range would give additional value to the data. Optical design where the optical path for both laser beam and returning signal light is mostly the same would eliminate multiple problems allowing a simpler overall optics design and making the final system thus more robust as in our alternative design 2 presented below. This can be achieved with the use of a dichroic filter transparent to the laser wavelength but reflecting all other wavelengths or with a mirror with a hole for the laser beam.

Alternative design 1 is presented in figure 9.1. In this design both the focus and receiver optics are put onto one discrete optics module that turns in two directions. The laser beam always comes from same orientation in to the module because of two mirrors that turning together with the module directing the beam. Advantage compared to design 1 is that only a smaller and lighter part of system needs to move for the scanning. Focus and receiver are still on separate optical paths, but the laser doesn't need to be turned anymore.

Alternative design 2 is presented in figure 9.2. This design has the same optical path for both laser and signal and scanning is done with two scanning mirrors. Either a dichroic mirror or a mirror with a hole cut through allows the laser beam pass while redirecting the signal light. In this design the only moving parts are the scanning mirrors. It makes scanning a lighter process and allows for faster scanning, which is a big advantage for this design. Important problem to consider in this design is how much of the signal light can effectively be gathered through the two scanning mirrors. An example of similar design used previously for hyperspectral scanning is described and pictured in a paper [97] by Hakala et al.

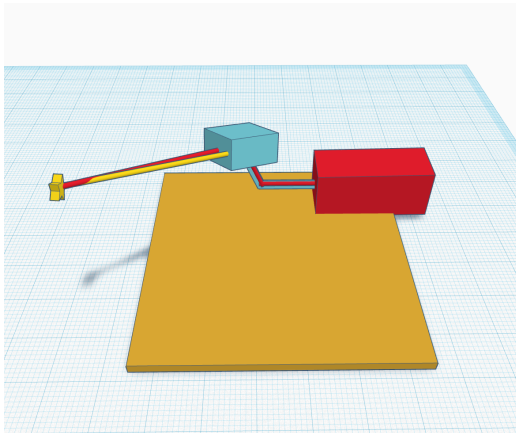


Figure 9.1: Alternative design 1 model with separated turning optics module

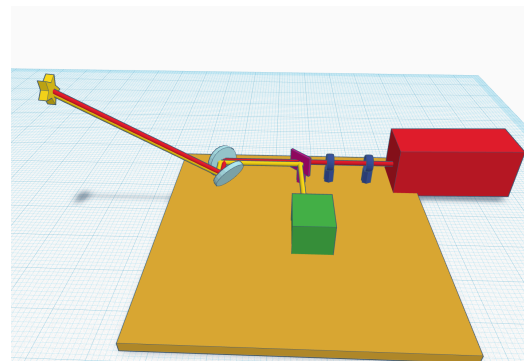


Figure 9.2: Alternative design 2 model with scanning mirrors

9.6 Acknowledgements

The results presented here is the output of many people working together. People and organizations that contributed to this project are in no particular order: Tuure Takala, Henri Johansson, Konstantinos Bis, Ari Hartikainen, Lasse Kangas, Jussi Leveinen, Otto Hedström, Jorma Palmén and LaDiMo Oy, Agnico Eagle Mines Limited, Aalto

University Department of Civil Engineering staff, Aalto Design Factory staff.

There are others not named here who worked on the project, supported and helped us and deserve thanks. One specific part where the true author needs to be pointed out is that Tuure Takala is responsible for the design and 3D models in figures 5.3 and 5.4 and in appendix A. Special thanks is given to Agnico Eagle mines for providing us with samples used in this work.

Funding for this work came from project funding from Academy of Finland and Challenge Finland competition of TEKES. The author reports no conflicts of interest.

9.7 Source repository

The scripts, models and data produced during this project are published at Zenodo under digital object identifier DOI:10.5281/zenodo.2620002 and are available at <https://doi.org/10.5281/zenodo.2620002>. The thesis text and 3D models are licensed under Creative Commons Attribution 4.0 International Licenses CC-BY 4.0 and the codes and experimental data are public domain released under CC0. Some used instruments, notably our spectrometers, have only proprietary drivers available which we cannot share.

Important note for anyone considering to look into this repository is that the code is not well made or documented and should not be used as is in any application. We give no guarantee to the code or even if it does what it claims to do. It is published as respecting the ideals of open research striving for easier reproduction of our results, and as a source of ideas for those working on similar projects.

References

- [1] S. Maurice, R. C. Wiens, M. Saccoccio, B. Barraclough, O. Gasnault, O. Forni, N. Mangold, D. Baratoux, S. Bender, G. Berger, J. Bernardin, M. Berthé, N. Bridges, D. Blaney, M. Bouyé, P. Caïs, B. Clark, S. Clegg, A. Cousin, D. Cremers, A. Cros, L. DeFlores, C. Derycke, B. Dingler, G. Dromart, B. Dubois, M. Dupieux, E. Durand, L. d’Uston, C. Fabre, B. Faure, A. Gaboriaud, T. Gharsa, K. Herkenhoff, E. Kan, L. Kirkland, D. Kouach, J.-L. Lacour, Y. Langevin, J. Lasue, S. L. Mouélic, M. Lescure, E. Lewin, D. Limonadi, G. Manhès, P. Mauchien, C. McKay, P.-Y. Meslin, Y. Michel, E. Miller, H. E. Newsom, G. Orttner, A. Paillet, L. Parès, Y. Parot, R. Pérez, P. Pinet, F. Poitrasson, B. Quertier, B. Sallé, C. Sotin, V. Sautter, H. Séran, J. J. Simmonds, J.-B. Sirven, R. Stiglich, N. Striebig, J.-J. Thocaven, M. J. Toplis, and D. Vaniman, “[The ChemCam Instrument Suite on the Mars Science Laboratory \(MSL\) Rover: Science Objectives and Mast Unit Description](#),” *Space Science Reviews*, vol. 170, no. 1-4, pp. 95–166, Sep. 2012. doi: 10.1007/s11214-012-9912-2
- [2] R. C. Wiens, S. Maurice, B. Barraclough, M. Saccoccio, W. C. Barkley, J. F. Bell, S. Bender, J. Bernardin, D. Blaney, J. Blank, M. Bouyé, N. Bridges, N. Bultman, P. Caïs, R. C. Clanton, B. Clark, S. Clegg, A. Cousin, D. Cremers, A. Cros, L. DeFlores, D. Delapp, R. Dingler, C. D’Uston, M. D. Dyar, T. Elliott, D. Enemark, C. Fabre, M. Flores, O. Forni, O. Gasnault, T. Hale, C. Hays, K. Herkenhoff, E. Kan, L. Kirkland, D. Kouach, D. Landis, Y. Langevin, N. Lanza, F. LaRocca, J. Lasue, J. Latino, D. Limonadi, C. Lindensmith, C. Little, N. Mangold, G. Manhes, P. Mauchien, C. McKay, E. Miller, J. Mooney, R. V. Morris, L. Morrison, T. Nelson, H. Newsom, A. Ollila, M. Ott, L. Pares, R. Perez, F. Poitrasson, C. Provost, J. W. Reiter, T. Roberts, F. Romero, V. Sautter, S. Salazar, J. J. Simmonds, R. Stiglich, S. Storms, N. Striebig, J.-J. Thocaven, T. Trujillo, M. Ulibarri, D. Vaniman, N. Warner, R. Waterbury, R. Whitaker, J. Witt, and B. Wong-Swanson, “[The ChemCam Instrument Suite on the Mars Science Laboratory \(MSL\) Rover: Body Unit and Combined System Tests](#),” *Space Science Reviews*, vol. 170, no. 1-4, pp. 167–227, Sep. 2012. doi: 10.1007/s11214-012-9902-4
- [3] R. Noll, *Laser-Induced Breakdown Spectroscopy*. Berlin, Heidelberg: Springer Berlin Heidelberg, 2012. ISBN 978-3-642-20667-2 978-3-642-20668-9
- [4] M. Bertolotti, *The History of the Laser*. Bristol ; Philadelphia: Institute of Physics Pub, 2005. ISBN 978-0-7503-0911-0 OCLC: ocm56966050.
- [5] Radziemski, *Lasers-Induced Plasmas and Applications*. CRC Press, Jun. 1989. ISBN 978-0-8247-8078-4
- [6] J.-G. Son, Y. Lee, and D.-K. Ko, “[Signal enhancement of laser-induced breakdown spectroscopy by applying synchronized buffer gas pulses](#),”

- Applied Physics Express*, vol. 11, no. 10, p. 102401, Oct. 2018. doi: 10.7567/APEX.11.102401
- [7] S. Zhang, X. Wang, M. He, Y. Jiang, B. Zhang, W. Hang, and B. Huang, “[Laser-induced plasma temperature](#),” *Spectrochimica Acta Part B: Atomic Spectroscopy*, vol. 97, pp. 13–33, Jul. 2014. doi: 10.1016/j.sab.2014.04.009
- [8] R. S. Harmon, R. E. Russo, and R. R. Hark, “[Applications of laser-induced breakdown spectroscopy for geochemical and environmental analysis: A comprehensive review](#),” *Spectrochimica Acta Part B: Atomic Spectroscopy*, vol. 87, pp. 11–26, Sep. 2013. doi: 10.1016/j.sab.2013.05.017
- [9] R. S. Adrain and J. Watson, “[Laser microspectral analysis: A review of principles and applications](#),” *Journal of Physics D: Applied Physics*, vol. 17, no. 10, pp. 1915–1940, Oct. 1984. doi: 10.1088/0022-3727/17/10/004
- [10] S. Qiao, Y. Ding, D. Tian, L. Yao, and G. Yang, “[A Review of Laser-Induced Breakdown Spectroscopy for Analysis of Geological Materials](#),” *Applied Spectroscopy Reviews*, vol. 50, no. 1, pp. 1–26, Jan. 2015. doi: 10.1080/05704928.2014.911746
- [11] A. Kramida, Y. Ralchenko, J. Reader, and N. A. Team, “Atomic Spectra Database,” 2018. [Online]. Available: <https://physics.nist.gov/asd>
- [12] A. Ciucci, M. Corsi, V. Palleschi, S. Rastelli, A. Salvetti, and E. Tognoni, “[New Procedure for Quantitative Elemental Analysis by Laser-Induced Plasma Spectroscopy](#),” *Applied Spectroscopy*, vol. 53, no. 8, pp. 960–964, Aug. 1999. doi: 10.1366/0003702991947612
- [13] C. A. Smith, M. A. Martinez, D. K. Veirs, and D. A. Cremers, “[Pu-239/Pu-240 isotope ratios determined using high resolution emission spectroscopy in a laser-induced plasma](#),” *Spectrochimica Acta Part B: Atomic Spectroscopy*, vol. 57, no. 5, pp. 929–937, May 2002. doi: 10.1016/S0584-8547(02)00023-X
- [14] R. E. Russo, A. A. Bol’shakov, X. Mao, C. P. McKay, D. L. Perry, and O. Sorkhabi, “[Laser Ablation Molecular Isotopic Spectrometry](#),” *Spectrochimica Acta Part B: Atomic Spectroscopy*, vol. 66, no. 2, pp. 99–104, Feb. 2011. doi: 10.1016/j.sab.2011.01.007
- [15] N. Khajehzadeh, “[Analytical techniques for online mineral identification](#),” PhD Thesis, Aalto university, 2018.
- [16] S.-L. Lui and A. Koujelev, “[Accurate identification of geological samples using artificial neural network processing of laser-induced breakdown spectroscopy data](#),” *Journal of Analytical Atomic Spectrometry*, vol. 26, no. 12, p. 2419, 2011. doi: 10.1039/c1ja10093a

- [17] A. Giakoumaki, I. Osticioli, and D. Anglos, “Spectroscopic analysis using a hybrid LIBS-Raman system,” *Applied Physics A*, vol. 83, no. 4, pp. 537–541, Jun. 2006. doi: 10.1007/s00339-006-3541-0
- [18] M. Hoehse, A. Paul, I. Gornushkin, and U. Panne, “Multivariate classification of pigments and inks using combined Raman spectroscopy and LIBS,” *Analytical and Bioanalytical Chemistry*, vol. 402, no. 4, pp. 1443–1450, Feb. 2012. doi: 10.1007/s00216-011-5287-6
- [19] R. C. Wiens, S. K. Sharma, J. Thompson, A. Misra, and P. G. Lucey, “Joint analyses by laser-induced breakdown spectroscopy (LIBS) and Raman spectroscopy at stand-off distances,” *Spectrochimica Acta Part A: Molecular and Biomolecular Spectroscopy*, vol. 61, no. 10, pp. 2324–2334, Aug. 2005. doi: 10.1016/j.saa.2005.02.031
- [20] S. K. Sharma, A. K. Misra, P. G. Lucey, and R. C. Lentz, “A combined remote Raman and LIBS instrument for characterizing minerals with 532nm laser excitation,” *Spectrochimica Acta Part A: Molecular and Biomolecular Spectroscopy*, vol. 73, no. 3, pp. 468–476, Aug. 2009. doi: 10.1016/j.saa.2008.08.005
- [21] J. Moros, J. A. Lorenzo, P. Lucena, L. Miguel Tobaría, and J. J. Laserna, “Simultaneous Raman Spectroscopy-Laser-Induced Breakdown Spectroscopy for Instant Standoff Analysis of Explosives Using a Mobile Integrated Sensor Platform,” *Analytical Chemistry*, vol. 82, no. 4, pp. 1389–1400, Feb. 2010. doi: 10.1021/ac902470v
- [22] F. Hilbk-Kortenbruck, R. Noll, P. Wintjens, H. Falk, and C. Becker, “Analysis of heavy metals in soils using laser-induced breakdown spectrometry combined with laser-induced fluorescence,” *Atomic Spectroscopy*, vol. 56, no. 6, p. 13, 2001. doi: 10.1016/S0584-8547(01)00213-0
- [23] J. Li, Z. Hao, N. Zhao, R. Zhou, R. Yi, S. Tang, L. Guo, X. Li, X. Zeng, and Y. Lu, “Spatially selective excitation in laser-induced breakdown spectroscopy combined with laser-induced fluorescence,” *Optics Express*, vol. 25, no. 5, p. 4945, Mar. 2017. doi: 10.1364/OE.25.004945
- [24] J. Kang, R. Li, Y. Wang, Y. Chen, and Y. Yang, “Ultrasensitive detection of trace amounts of lead in water by LIBS-LIF using a wood-slice substrate as a water absorber,” *Journal of Analytical Atomic Spectrometry*, vol. 32, no. 11, pp. 2292–2299, 2017. doi: 10.1039/C7JA00244K
- [25] J. D. Hybl, S. M. Tysk, S. R. Berry, and M. P. Jordan, “Laser-induced fluorescence-cued, laser-induced breakdown spectroscopy biological-agent detection,” *Applied Optics*, vol. 45, no. 34, p. 8806, Dec. 2006. doi: 10.1364/AO.45.008806

- [26] H. Loudyi, K. Rifai, S. Laville, F. Vidal, M. Chaker, and M. Sabsabi, "Improving laser-induced breakdown spectroscopy (LIBS) performance for iron and lead determination in aqueous solutions with laser-induced fluorescence (LIF)," *Journal of Analytical Atomic Spectrometry*, vol. 24, no. 10, p. 1421, 2009. doi: 10.1039/b909485g
- [27] G. S. Senesi, "Laser-Induced Breakdown Spectroscopy (LIBS) applied to terrestrial and extraterrestrial analogue geomaterials with emphasis to minerals and rocks," *Earth-Science Reviews*, vol. 139, pp. 231–267, Dec. 2014. doi: 10.1016/j.earscirev.2014.09.008
- [28] D. A. Cremers and L. J. Radziemski, *Handbook of Laser-Induced Breakdown Spectroscopy*. John Wiley & Sons, Mar. 2013. ISBN 978-1-118-56736-4
- [29] F. R. Doucet, G. Lithgow, R. Kosierb, P. Bouchard, and M. Sabsabi, "Determination of isotope ratios using Laser-Induced Breakdown Spectroscopy in ambient air at atmospheric pressure for nuclear forensics," *Journal of Analytical Atomic Spectrometry*, vol. 26, no. 3, p. 536, 2011. doi: 10.1039/c0ja00199f
- [30] R. González, P. Lucena, L. M. Tobaría, and J. J. Laserna, "Standoff LIBS detection of explosive residues behind a barrier," *Journal of Analytical Atomic Spectrometry*, vol. 24, no. 8, p. 1123, 2009. doi: 10.1039/b821566a
- [31] J. L. Gottfried, F. C. De Lucia Jr., and A. W. Miziolek, "Discrimination of explosive residues on organic and inorganic substrates using laser-induced breakdown spectroscopy," *Journal of Analytical Atomic Spectrometry*, vol. 24, no. 3, p. 288, 2009. doi: 10.1039/b818481j
- [32] F. C. De Lucia, Jr., J. L. Gottfried, C. A. Munson, and A. W. Miziolek, "Multivariate analysis of standoff laser-induced breakdown spectroscopy spectra for classification of explosive-containing residues," *Applied Optics*, vol. 47, no. 31, p. G112, Nov. 2008. doi: 10.1364/AO.47.00G112
- [33] J. A. Stearns, S. E. McElman, and J. A. Dodd, "Identification of vapor-phase chemical warfare agent simulants and rocket fuels using laser-induced breakdown spectroscopy," *Applied Optics*, vol. 49, no. 13, p. C8, May 2010. doi: 10.1364/AO.49.0000C8
- [34] J. Diedrich, S. J. Rehse, and S. Palchaudhuri, "*Escherichia Coli* identification and strain discrimination using nanosecond laser-induced breakdown spectroscopy," *Applied Physics Letters*, vol. 90, no. 16, p. 163901, Apr. 2007. doi: 10.1063/1.2723659
- [35] J. Diedrich, S. J. Rehse, and S. Palchaudhuri, "Pathogenic *Escherichia coli* strain discrimination using laser-induced breakdown spectroscopy," *Journal of Applied Physics*, vol. 102, no. 1, p. 014702, Jul. 2007. doi: 10.1063/1.2752784

- [36] M. R. Martelli, F. Brygo, A. Sadoudi, P. Delaporte, and C. Barron, “[Laser-Induced Breakdown Spectroscopy and Chemometrics: A Novel Potential Method to Analyze Wheat Grains](#),” *Journal of Agricultural and Food Chemistry*, vol. 58, no. 12, pp. 7126–7134, Jun. 2010. doi: 10.1021/jf100665u
- [37] G. Bilge, H. M. Velioglu, B. Sezer, K. E. Eseller, and I. H. Boyaci, “[Identification of meat species by using laser-induced breakdown spectroscopy](#),” *Meat Science*, vol. 119, pp. 118–122, Sep. 2016. doi: 10.1016/j.meatsci.2016.04.035
- [38] H. Balzer, S. Hölters, V. Sturm, and R. Noll, “[Systematic line selection for online coating thickness measurements of galvanised sheet steel using LIBS](#),” *Analytical and Bioanalytical Chemistry*, vol. 385, no. 2, pp. 234–239, Apr. 2006. doi: 10.1007/s00216-006-0348-y
- [39] M. Z. Martin, N. Labbé, N. André, S. D. Wullschleger, R. D. Harris, and M. H. Ebinger, “[Novel Multivariate Analysis for Soil Carbon Measurements Using Laser-Induced Breakdown Spectroscopy](#),” *Soil Science Society of America Journal*, vol. 74, no. 1, p. 87, 2010. doi: 10.2136/sssaj2009.0102
- [40] R. M. da Silva, D. M. Milori, E. C. Ferreira, E. J. Ferreira, F. J. Krug, and L. Martin-Neto, “[Total carbon measurement in whole tropical soil sample](#),” *Spectrochimica Acta Part B: Atomic Spectroscopy*, vol. 63, no. 10, pp. 1221–1224, Oct. 2008. doi: 10.1016/j.sab.2008.09.003
- [41] O. Samek, M. Liška, J. Kaiser, D. Beddows, H. Telle, and S. Kukhlevsky, “[Clinical Application of Laser-Induced Breakdown Spectroscopy to the Analysis of Teeth and Dental Materials](#),” *Journal of Clinical Laser Medicine & Surgery*, vol. 18, no. 6, pp. 281–289, Dec. 2000. doi: 10.1089/clm.2000.18.281
- [42] A. Kumar, F.-Y. Yueh, J. P. Singh, and S. Burgess, “[Characterization of malignant tissue cells by laser-induced breakdown spectroscopy](#),” *Applied Optics*, vol. 43, no. 28, p. 5399, Oct. 2004. doi: 10.1364/AO.43.005399
- [43] I. V. Akhtyrchenko, E. Beliaev, I. P. Vysotskii, O. Garin, A. Godlevskii, V. Zuev, I. D. Kopytin, A. Kuriapin, V. Pogodaev, and V. Pokasov, “Nonlinear energy attenuation of pulsed CO₂ laser radiation in the atmospheric surface layer,” *Fizika*, vol. 26, pp. 5–13, 1983.
- [44] K. Stelmaszczyk, P. Rohwetter, G. Méjean, J. Yu, E. Salmon, J. Kasparian, R. Ackermann, J.-P. Wolf, and L. Wöste, “[Long-distance remote laser-induced breakdown spectroscopy using filamentation in air](#),” *Applied Physics Letters*, vol. 85, no. 18, pp. 3977–3979, Nov. 2004. doi: 10.1063/1.1812843
- [45] B. Sallé, P. Mauchien, and S. Maurice, “[Laser-Induced Breakdown Spectroscopy in open-path configuration for the analysis of distant objects](#),” *Spectrochimica Acta Part B: Atomic Spectroscopy*, vol. 62, no. 8, pp. 739–768, Aug. 2007. doi: 10.1016/j.sab.2007.07.001

- [46] R. Grönlund, M. Lundqvist, and S. Svanberg, “Remote imaging laser-induced breakdown spectroscopy and remote cultural heritage ablative cleaning,” *Optics Letters*, vol. 30, no. 21, p. 2882, Nov. 2005. doi: 10.1364/OL.30.002882
- [47] R. Grönlund, M. Lundqvist, and S. Svanberg, “Remote Imaging Laser-Induced Breakdown Spectroscopy and Laser-Induced Fluorescence Spectroscopy Using Nanosecond Pulses from a Mobile Lidar System,” *Applied Spectroscopy*, vol. 60, no. 8, pp. 853–859, Aug. 2006. doi: 10.1366/000370206778062138
- [48] P. Weibring, H. Edner, and S. Svanberg, “Versatile mobile lidar system for environmental monitoring,” *Applied Optics*, vol. 42, no. 18, p. 3583, Jun. 2003. doi: 10.1364/AO.42.003583
- [49] P. J. Treado, M. P. Nelson, and H. City, “Time and space resolved standoff hyperspectral IED explosives lidar detection,” U.S. Patent US8 054 454B2, 2010.
- [50] N. Khajehzadeh and T. K. Kauppinen, “Fast mineral identification using elemental LIBS technique,” *IFAC-PapersOnLine*, vol. 48, no. 17, pp. 119–124, 2015. doi: 10.1016/j.ifacol.2015.10.089
- [51] N. Khajehzadeh, O. Haavisto, and L. Koresaar, “On-stream and quantitative mineral identification of tailing slurries using LIBS technique,” *Minerals Engineering*, vol. 98, pp. 101–109, Nov. 2016. doi: 10.1016/j.mineng.2016.08.002
- [52] N. Khajehzadeh, O. Haavisto, and L. Koresaar, “On-stream mineral identification of tailing slurries of an iron ore concentrator using data fusion of LIBS, reflectance spectroscopy and XRF measurement techniques,” *Minerals Engineering*, vol. 113, pp. 83–94, Nov. 2017. doi: 10.1016/j.mineng.2017.08.007
- [53] “Outotec Courier 8 SL analyzer,” Apr. 2019. [Online]. Available: <https://www.outotec.com/products/analyzers-and-automation/courier-8-sl-analyzer/>
- [54] “ELEMISION Mission Coriosity,” Apr. 2019. [Online]. Available: https://www.elemision.ca/en/products.php?#mission_coriosity
- [55] K. Rifai, F. Doucet, L. Özcan, and F. Vidal, “LIBS core imaging at kHz speed: Paving the way for real-time geochemical applications,” *Spectrochimica Acta Part B: Atomic Spectroscopy*, vol. 150, pp. 43–48, Dec. 2018. doi: 10.1016/j.sab.2018.10.007
- [56] “Maya Laser Online elemental analyzer,” Apr. 2019. [Online]. Available: <http://www.laser-distance-spectrometry.com/pages/index/en.php>
- [57] E. B. Coindre, C. Elie, J. Goujon, A. Fortas, O. Musset, and F. Fariaut, “EasyLIBS, a new portable LIBS system,” in *LIBS 2008*, no. paper GTP6, 2008, p. Poster.

- [58] A. Mezzacappa, N. Melikechi, A. Cousin, R. Wiens, J. Lasue, S. Clegg, R. Tokar, S. Bender, N. Lanza, S. Maurice, G. Berger, O. Forni, O. Gasnault, M. Dyar, T. Boucher, E. Lewin, and C. Fabre, “[Application of distance correction to ChemCam laser-induced breakdown spectroscopy measurements,](#)” *Spectrochimica Acta Part B: Atomic Spectroscopy*, vol. 120, pp. 19–29, Jun. 2016. doi: 10.1016/j.sab.2016.03.009
- [59] L. Sun and H. Yu, “[Correction of self-absorption effect in calibration-free laser-induced breakdown spectroscopy by an internal reference method,](#)” *Talanta*, vol. 79, no. 2, pp. 388–395, Jul. 2009. doi: 10.1016/j.talanta.2009.03.066
- [60] T. Takahashi and B. Thornton, “[Quantitative methods for compensation of matrix effects and self-absorption in Laser Induced Breakdown Spectroscopy signals of solids,](#)” *Spectrochimica Acta Part B: Atomic Spectroscopy*, vol. 138, pp. 31–42, Dec. 2017. doi: 10.1016/j.sab.2017.09.010
- [61] S. M. Clegg, E. Sklute, M. D. Dyar, J. E. Barefield, and R. C. Wiens, “[Multivariate analysis of remote laser-induced breakdown spectroscopy spectra using partial least squares, principal component analysis, and related techniques,](#)” *Spectrochimica Acta Part B: Atomic Spectroscopy*, vol. 64, no. 1, pp. 79–88, Jan. 2009. doi: 10.1016/j.sab.2008.10.045
- [62] C. López-Moreno, S. Palanco, and J. J. Laserna, “[Remote laser-induced plasma spectrometry for elemental analysis of samples of environmental interest,](#)” *J. Anal. At. Spectrom.*, vol. 19, no. 11, pp. 1479–1484, 2004. doi: 10.1039/B408534E
- [63] J. M. Vadillo, P. L. García, S. Palanco, D. Romero, J. M. Baena, and J. J. Laserna, “[Remote, real-time, on-line monitoring of high-temperature samples by noninvasive open-path laser plasma spectrometry,](#)” *Analytical and Bioanalytical Chemistry*, vol. 375, no. 8, pp. 1144–1147, Apr. 2003. doi: 10.1007/s00216-003-1820-6
- [64] S. Palanco, C. López-Moreno, and J. J. Laserna, “[Design, construction and assessment of a field-deployable laser-induced breakdown spectrometer for remote elemental sensing,](#)” *Spectrochimica Acta Part B: Atomic Spectroscopy*, vol. 61, no. 1, pp. 88–95, Jan. 2006. doi: 10.1016/j.sab.2005.12.004
- [65] S. Palanco, S. Conesa, and J. J. Laserna, “[Analytical control of liquid steel in an induction melting furnace using a remote laser induced plasma spectrometer,](#)” *Journal of Analytical Atomic Spectrometry*, vol. 19, no. 4, p. 462, 2004. doi: 10.1039/b400354c
- [66] D. C. S. Beddows, “[Application of laser-induced breakdown spectroscopy to in situ analysis of liquid samples,](#)” *Optical Engineering*, vol. 39, no. 8, p. 2248, Aug. 2000. doi: 10.1117/1.1304855

- [67] D. F. Fornetti, *Instrumentation Control, Data Acquisition and Processing with MATLAB®*. Explore RF Ltd, 2013, vol. 2013. ISBN 978-0-9576635-3-4
- [68] M. Soltero, J. Zhang, and C. Cockril, “RS-422 and RS-485 Standards Overview and System Configurations,” Texas Instruments, Application Report, 2002.
- [69] “Modbus Application Protocol Specification V1.1b3,” 2012. [Online]. Available: http://www.modbus.org/docs/Modbus_Application_Protocol_V1_1b3.pdf
- [70] V. S. Alliance, “The VISA Library Specification VPP-4.3,” Oct. 2018.
- [71] P. Hariharan, *Basics of Interferometry*, 2nd ed. Amsterdam ; Boston: Elsevier Academic Press, 2007. ISBN 978-0-12-373589-8 OCLC: ocm70158467.
- [72] P. D. Barnett, N. Lamsal, and S. M. Angel, “Standoff Laser-Induced Breakdown Spectroscopy (LIBS) Using a Miniature Wide Field of View Spatial Heterodyne Spectrometer with Sub-Microsteradian Collection Optics,” *Applied Spectroscopy*, vol. 71, no. 4, pp. 583–590, Apr. 2017. doi: 10.1177/0003702816687569
- [73] F. Pomerleau, F. Colas, and R. Siegwart, “A Review of Point Cloud Registration Algorithms for Mobile Robotics,” *Foundations and Trends in Robotics*, vol. 4, no. 1, pp. 1–104, 2015. doi: 10.1561/23000000035
- [74] P. J. Besl and N. D. McKay, “Method for registration of 3-D shapes,” in *Robotics - DL Tentative*, P. S. Schenker, Ed., Boston, MA, Apr. 1992. doi: 10.1117/12.57955 pp. 586–606.
- [75] H. Chui and A. Rangarajan, “A new point matching algorithm for non-rigid registration,” *Computer Vision and Image Understanding*, vol. 89, no. 2-3, pp. 114–141, Feb. 2003. doi: 10.1016/S1077-3142(03)00009-2
- [76] Y. Tsing and T. Kanade, “A Correlation-Based Approach to Robust Point Set Registration,” in *Computer Vision - ECCV 2004*, T. Kanade, J. Kittler, J. M. Kleinberg, F. Mattern, J. C. Mitchell, O. Nierstrasz, C. Pandu Rangan, B. Steffen, M. Sudan, D. Terzopoulos, D. Tygar, M. Y. Vardi, G. Weikum, T. Pajdla, and J. Matas, Eds. Berlin, Heidelberg: Springer Berlin Heidelberg, 2004, vol. 3023, pp. 558–569. ISBN 978-3-540-21982-8 978-3-540-24672-5
- [77] A. Myronenko, X. B. Song, and M. A. Carreira-Perpiñán, “Non-rigid point set registration: Coherent Point Drift,” in *Advances in Neural Information Processing Systems 19, Proceedings of the Twentieth Annual Conference on Neural Information Processing Systems, Vancouver, British Columbia, Canada, December 4-7, 2006*, 2006. ISBN 0-262-19568-2 pp. 1009–1016.
- [78] N. Amenta, S. Choi, and R. K. Kolluri, “The power crust, unions of balls, and the medial axis transform,” *Computational Geometry*, vol. 19, no. 2-3, pp. 127–153, Jul. 2001. doi: 10.1016/S0925-7721(01)00017-7

- [79] M. Kazhdan, M. Bolitho, and H. Hoppe, “Poisson Surface Reconstruction,” in *Eurographics Symposium on Geometry Processing*, 2006, p. 10.
- [80] H. Hoppe, T. DeRose, T. Duchamp, J. McDonald, and W. Stuetzle, *Surface Reconstruction from Unorganized Points*. ACM, 1992, vol. 26, no. 2.
- [81] A. Belyaev, M. Alexa, T. Darmstadt, G. Turk, and H.-P. Seidel, *Multi-Level Partition of Unity Implicits*, 2003.
- [82] R. B. Rusu and S. Cousins, “3d is here: Point cloud library (pcl),” in *Robotics and Automation (ICRA), 2011 IEEE International Conference On*. IEEE, 2011, pp. 1–4.
- [83] “CloudCompare (Version 2.X) [GPL software].” 2018. [Online]. Available: <http://www.cloudcompare.org/>
- [84] P. Cignoni, M. Callieri, M. Corsini, M. Dellepiane, F. Ganovelli, and G. Ranzuglia, “Meshlab: An open-source mesh processing tool.” in *Eurographics Italian Chapter Conference*, vol. 2008, 2008, pp. 129–136.
- [85] Z. Wang, L. Li, L. West, Z. Li, and W. Ni, “[Spectrum standardization for laser-induced breakdown spectroscopy measurements](#),” *arXiv preprint arXiv:1106.0583*, p. 21, Jun. 2011. doi: 10.1016/j.sab.2012.01.005
- [86] M. L. Najarian and R. C. Chinni, “[Temperature and Electron Density Determination on Laser-Induced Breakdown Spectroscopy \(LIBS\) Plasmas: A Physical Chemistry Experiment](#),” *Journal of Chemical Education*, vol. 90, no. 2, pp. 244–247, Feb. 2013. doi: 10.1021/ed3003385
- [87] L. van der Maaten and G. Hinton, “Visualizing data using t-SNE,” *Journal of machine learning research*, vol. 9, no. Nov, pp. 2579–2605, 2008.
- [88] L. McInnes, J. Healy, and J. Melville, “[UMAP: Uniform Manifold Approximation and Projection for Dimension Reduction](#),” *arXiv preprint arXiv:1802.03426*, Feb. 2018.
- [89] L. Liang, T. Zhang, K. Wang, H. Tang, X. Yang, X. Zhu, Y. Duan, and H. Li, “[Classification of steel materials by laser-induced breakdown spectroscopy coupled with support vector machines](#),” *Applied Optics*, vol. 53, no. 4, p. 544, Feb. 2014. doi: 10.1364/AO.53.000544
- [90] A. Koujelev, M. Sabsabi, V. Motto-Ros, S. Laville, and S. Lui, “[Laser-induced breakdown spectroscopy with artificial neural network processing for material identification](#),” *Planetary and Space Science*, vol. 58, no. 4, pp. 682–690, Mar. 2010. doi: 10.1016/j.pss.2009.06.022
- [91] K. Ghosh, A. Stuke, M. Todorović, P. B. Jørgensen, M. N. Schmidt, A. Vehtari, and P. Rinke, “[Deep Learning Spectroscopy: Neural Networks for Molecular Excitation Spectra](#),” *Advanced Science*, p. 1801367, Jan. 2019. doi: 10.1002/advs.201801367

- [92] S. Musazzi and U. Perini, Eds., *Laser-Induced Breakdown Spectroscopy: Theory and Applications*, ser. Springer Series in Optical Sciences. Berlin ; New York: Springer, 2014, no. Volume 182. ISBN 978-3-642-45084-6 OCLC: ocn864498361.
- [93] L. Badea, “StepperDriver [MIT licensed software] GitHub Repository,” 2015. [Online]. Available: <https://github.com/laurb9/StepperDriver>
- [94] “SFS-EN 207:2017 Personal eye-protection equipment - Filters and eye-protectors against laser radiation (laser eye-protectors),” Mar. 2017.
- [95] K. Bis, “Geometallurgical characterization of the Kittilä gold ore deposit,” Master’s Thesis, Aalto university, Dec. 2018.
- [96] J. O. Cáceres, F. Pelascini, V. Motto-Ros, S. Moncayo, F. Trichard, G. Panczer, A. Marín-Roldán, J. A. Cruz, I. Coronado, and J. Martín-Chivelet, “Megapixel multi-elemental imaging by Laser-Induced Breakdown Spectroscopy, a technology with considerable potential for paleoclimate studies,” *Scientific Reports*, vol. 7, no. 1, Dec. 2017. doi: 10.1038/s41598-017-05437-3
- [97] T. Hakala, J. Suomalainen, S. Kaasalainen, and Y. Chen, “Full waveform hyperspectral LiDAR for terrestrial laser scanning,” *Optics Express*, vol. 20, no. 7, p. 7119, Mar. 2012. doi: 10.1364/OE.20.007119

A 3D models and printable parts

Figures A1-A4 show 3D models for CNC parts of the device. The parts were made from a technical plastic polyoxymethylene(POM), also called polyacetal. Figures A5-A8 show 3D models of the 3D printed parts of the device. Important note is that not all of the 3D printed parts we made used are included here, particularly the optics receiver module. The 3D printed parts were printed with polylactic acid(PLA). Design of all of these is by Tuure Takala. The model files are available at Zenodo as described in main thesis section 9.7.

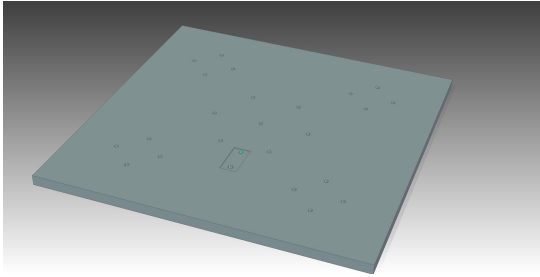


Figure A1: CNC machined part model for the tunnel scanner: base plate.

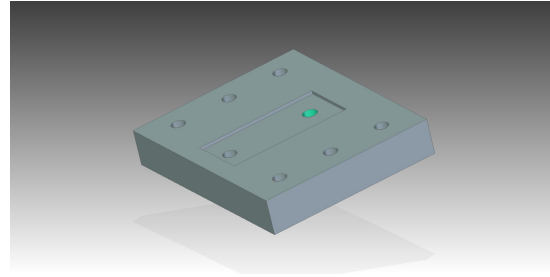


Figure A2: CNC machined parts model for the tunnel scanner: attachment.

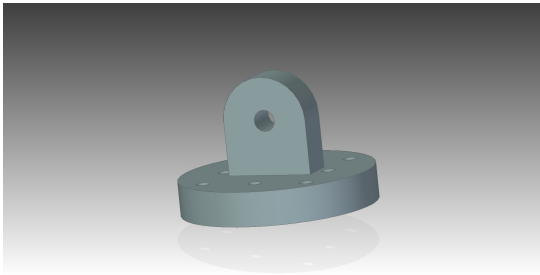


Figure A3: CNC machined part model for the tunnel scanner: knuckle joint upper.

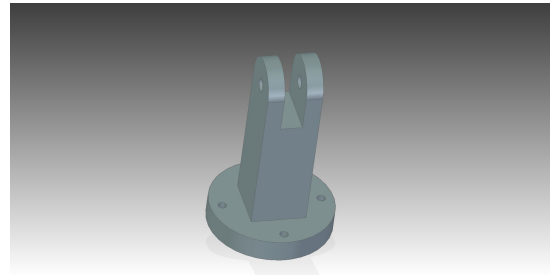


Figure A4: CNC machined part model for the tunnel scanner: knuckle joint lower.

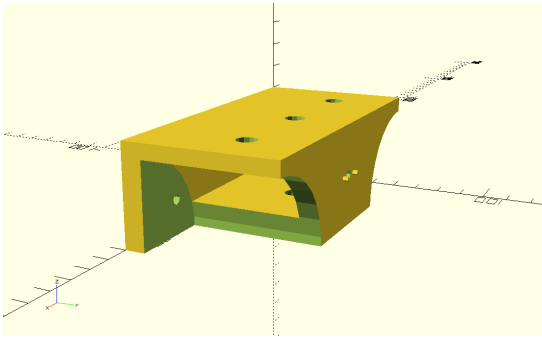


Figure A5: 3D printed parts for the optics system: back plate. Made with OpenSCAD.

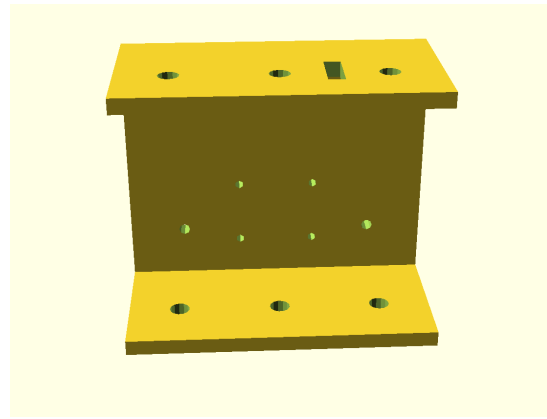


Figure A6: 3D printed parts for the optics system: focus motor holder. Made with OpenSCAD.

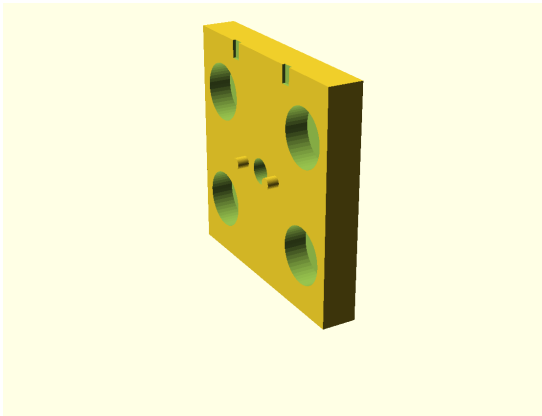


Figure A7: 3D printed parts for the optics system: cart part. Made with OpenSCAD.

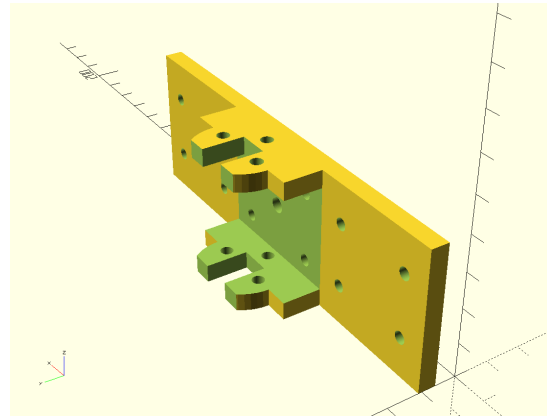


Figure A8: 3D printed parts for the optics system: focus cart. Made with OpenSCAD.

B Pictures of the prototype device

Figures B1-B3 are photograph of the prototype device.



Figure B1: Mobile tunnel wall LIBS scanner device without casing

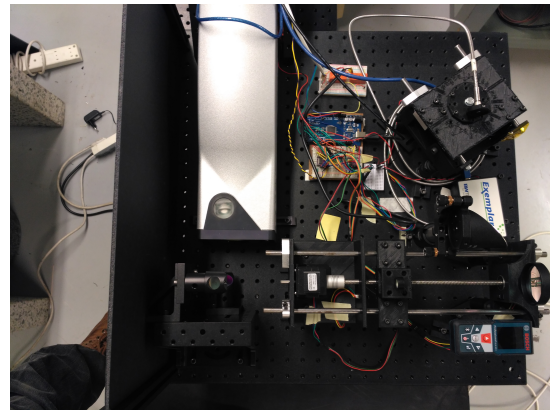


Figure B2: Mobile tunnel wall LIBS scanner device without casing seen from above

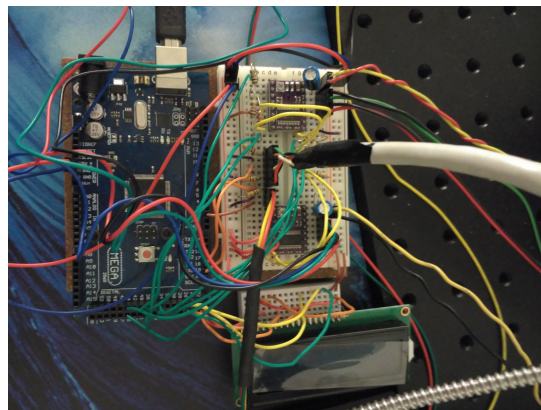


Figure B3: Microcontroller wiring

C Tunnel test results in detail

Figures C1-C28 show elemental heatmaps obtained from the tunnel test.

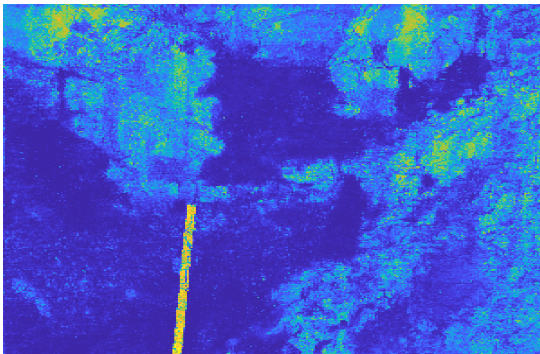


Figure C1: Tunnel wall elemental heatmap for aluminium. Combined from multiple wavelengths.

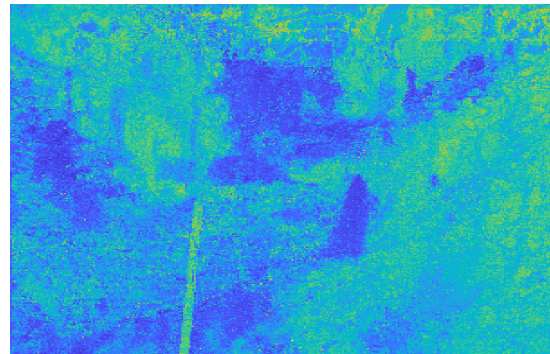


Figure C2: Tunnel wall elemental normalized heatmap for aluminium. Combined from multiple wavelengths.

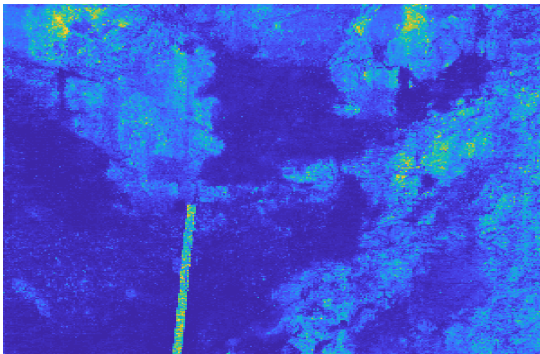


Figure C3: Tunnel wall elemental heatmap for calcium. Combined from multiple wavelengths.

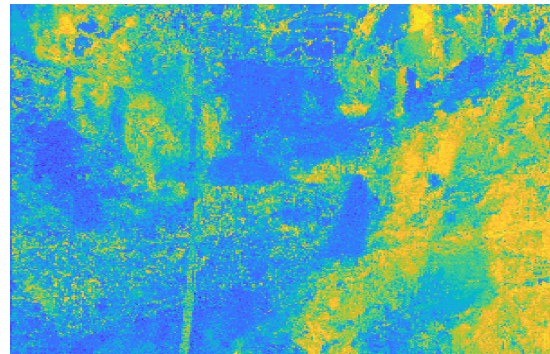


Figure C4: Tunnel wall elemental normalized heatmap for calcium. Combined from multiple wavelengths.

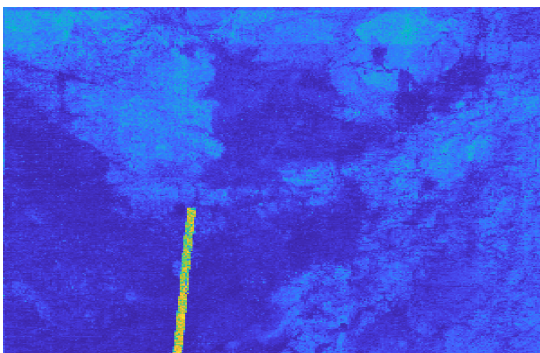


Figure C5: Tunnel wall elemental heatmap for hydrogen. Combined from multiple wavelengths.

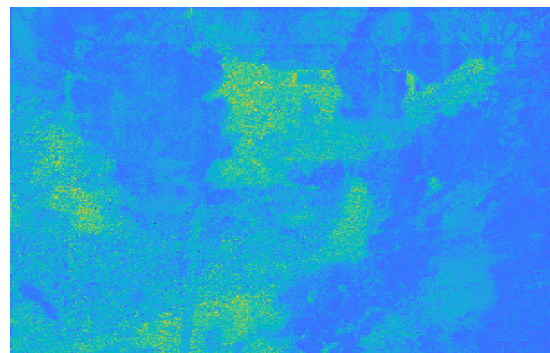


Figure C6: Tunnel wall elemental normalized heatmap for hydrogen. Combined from multiple wavelengths.

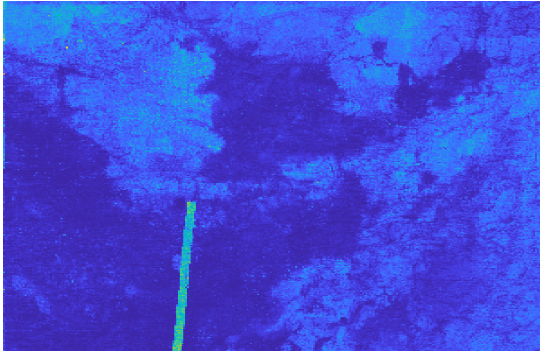


Figure C7: Tunnel wall elemental heatmap for iron. Combined from multiple wavelengths.

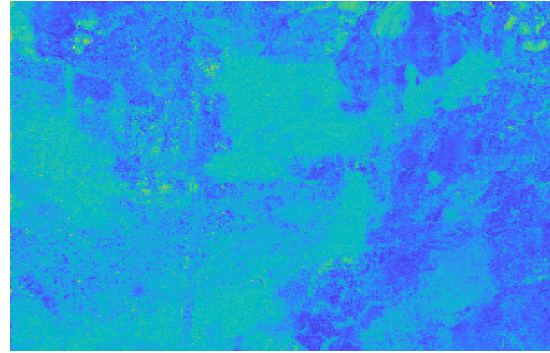


Figure C8: Tunnel wall elemental normalized heatmap for iron. Combined from multiple wavelengths.

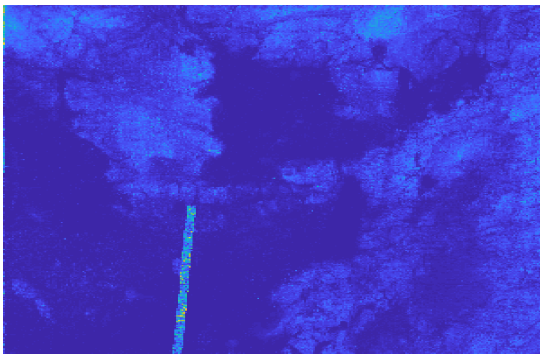


Figure C9: Tunnel wall elemental heatmap for potassium. Combined from multiple wavelengths.

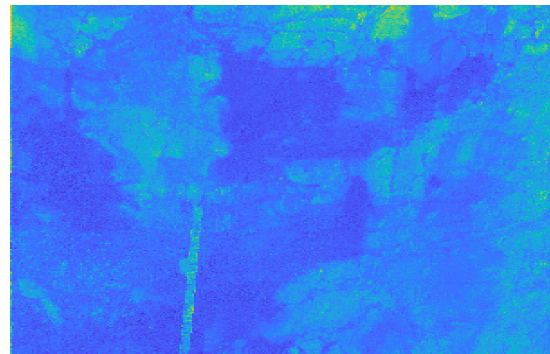


Figure C10: Tunnel wall elemental normalized heatmap for potassium. Combined from multiple wavelengths.

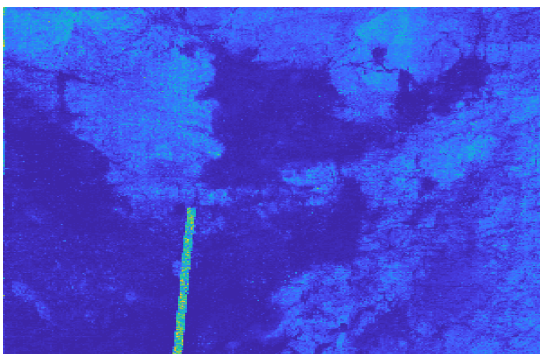


Figure C11: Tunnel wall elemental heatmap for magnesium. Combined from multiple wavelengths.

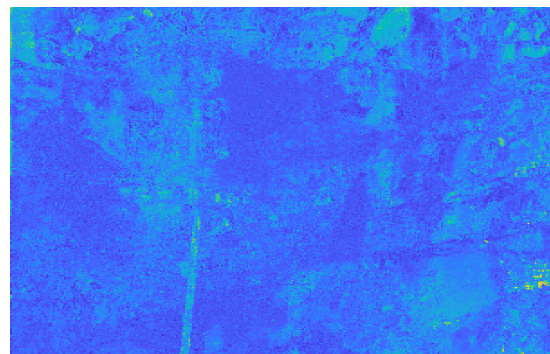


Figure C12: Tunnel wall elemental normalized heatmap for magnesium. Combined from multiple wavelengths.

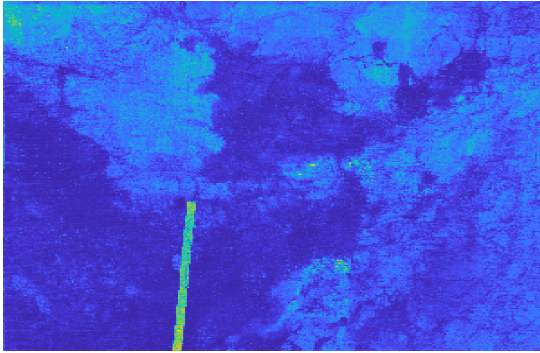


Figure C13: Tunnel wall elemental heatmap for manganese. Combined from multiple wavelengths.

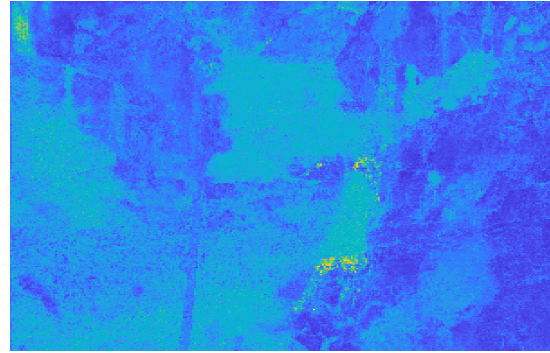


Figure C14: Tunnel wall elemental normalized heatmap for manganese. Combined from multiple wavelengths.

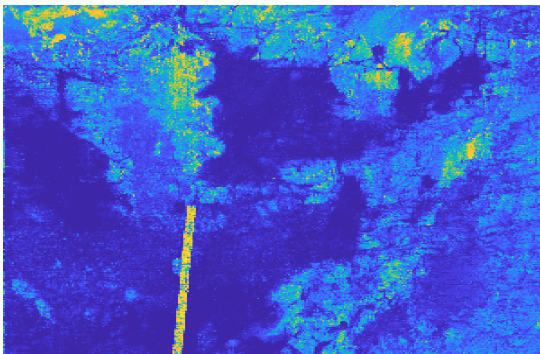


Figure C15: Tunnel wall elemental heatmap for sodium. Combined from multiple wavelengths.

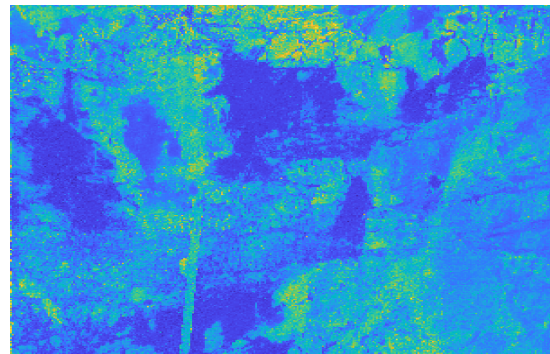


Figure C16: Tunnel wall elemental normalized heatmap for sodium. Combined from multiple wavelengths.

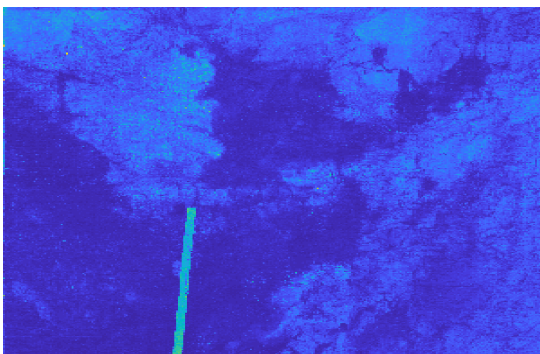


Figure C17: Tunnel wall elemental heatmap for nickel. Combined from multiple wavelengths.

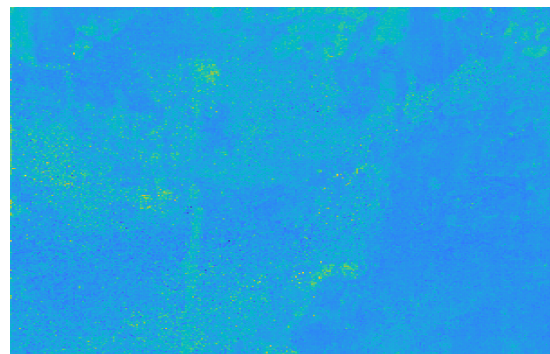


Figure C18: Tunnel wall elemental normalized heatmap for nickel. Combined from multiple wavelengths.

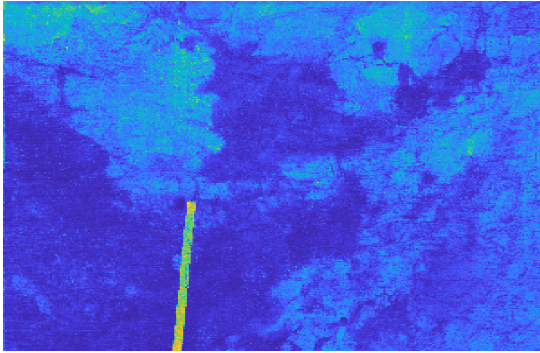


Figure C19: Tunnel wall elemental heatmap for nitrogen. Combined from multiple wavelengths.

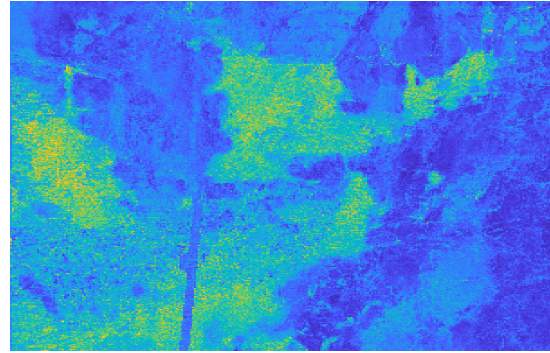


Figure C20: Tunnel wall elemental normalized heatmap for nitrogen. Combined from multiple wavelengths.

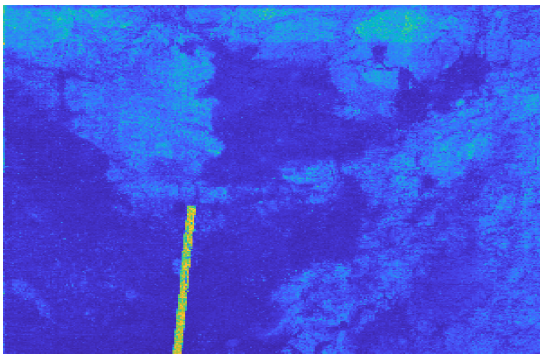


Figure C21: Tunnel wall elemental heatmap for oxygen. Combined from multiple wavelengths.

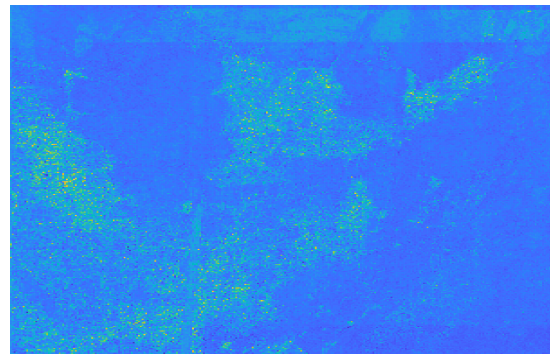


Figure C22: Tunnel wall elemental normalized heatmap for oxygen. Combined from multiple wavelengths.

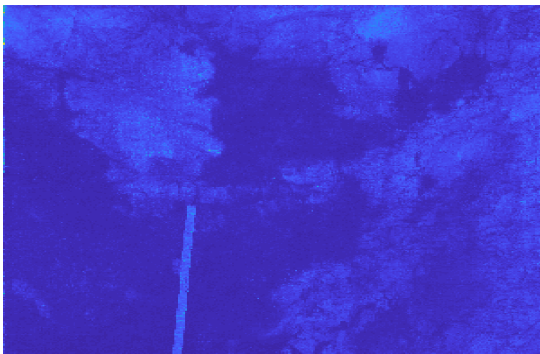


Figure C23: Tunnel wall elemental heatmap for rubidium. Combined from multiple wavelengths.

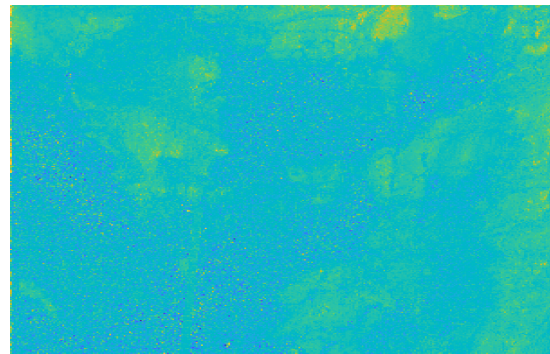


Figure C24: Tunnel wall elemental normalized heatmap for rubidium. Combined from multiple wavelengths.

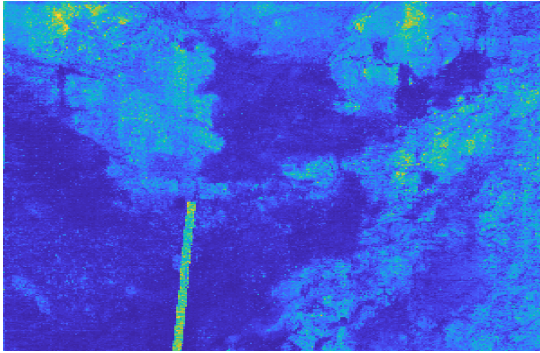


Figure C25: Tunnel wall elemental heatmap for silicon. Combined from multiple wavelengths.

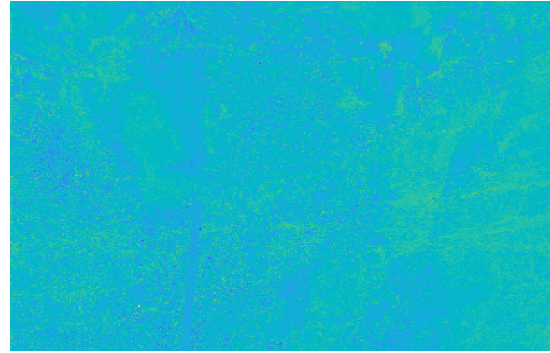


Figure C26: Tunnel wall elemental normalized heatmap for silicon. Combined from multiple wavelengths.

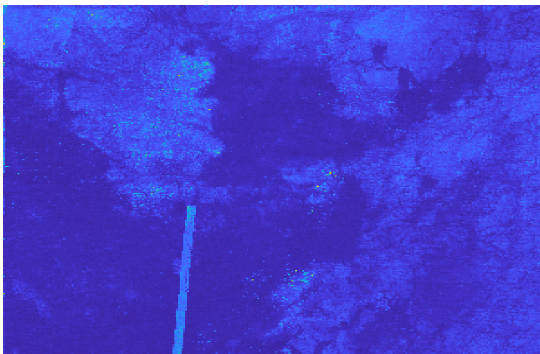


Figure C27: Tunnel wall elemental heatmap for titanium. Combined from multiple wavelengths.

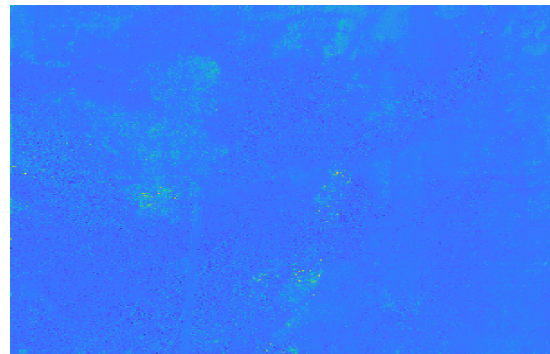


Figure C28: Tunnel wall elemental normalized heatmap for titanium. Combined from multiple wavelengths.